7

High-Order Numerical Methods for BiGlobal Flow Instability Analysis and Control

Javier de Vicente[1], Daniel Rodríguez[2], Leo González[3] and Vassilis Theofilis[4]
[1]*Department of Applied Mathematics and Statistic. School of Aeronautics, Universidad Politécnica de Madrid*
[2]*School of Aeronautics, Universidad Politécnica de Madrid*
[3]*School of Naval Engineering, Universidad Politécnica de Madrid*
[4]*School of Aeronautics, Universidad Politécnica de Madrid*
Spain

1. Introduction

In recent years flow instability and flow control research has focused attention on two novel and promising areas, investigation of perturbations in the limit of short times after their introduction into the flow Schmid & Henningson (2001) and study of modal and non-modal perturbations in complex, essentially non–parallel flows. A rather complete, up to that time, account of the rapidly growing latter area was discussed in Collis et al. (2004); Theofilis (2003); the role of (especially global) instability analysis in flow control is discussed elsewhere Theofilis (2009b). The present article deals with the theory and numerical aspects underlying the recent rapid developments in global instability research, in an attempt to generate a self–contained account of the areas in which the authors have been working in the last decade, as opposed to producing a review-type article on the many developments which have recently taken place.

When discussing numerical methods for the solution of the partial–derivative eigenvalue problem it is instructive to remind the reader of the process by which one arrives at the various large–scale eigenvalue problems solved in a global instability context; pictorially, this process is shown in the charts presented in figure 1. In the first of these decision trees, one is confronted with the temporal derivative in the linearized Navier–Stokes equations (LNSE) and the possibility to either discretize this term (in a so–called "time-stepping" approach), thereby solving for arbitrary temporal development of the perturbations (including transient growth) or work in frequency space by introducing eigenmodes, a procedure which is permissible by the separability of the temporal and spatial derivatives in the LNSE. Once this decision has been made, the next step is to deal with how to treat the LNSE matrix; there too, two paths may be followed, one ("Time-steppers") along which the matrix describing the evolution of perturbations is not formed explicitly and tools analogous with those used in direct numerical simulations are employed, and another one (Generalized Eigenvalue Problem – GEVP) along which the matrix (of leading dimension potentially reaching 1 Tb Kitsios et al. (2008)) is stored in (shared or distributed) memory. From the outset the question

may be posed as to which is the more appropriate path to be followed. The answer depends on whether one is interested in recovering only a few or many members of the eigenspectrum, time–steppers (alongside high–quality numerics) being appropriate for the first task, while solution to the GEVP provides access to a potentially large window of eigenmodes.

The chart of figure 1 ,in the lower case, in principle describes spatial discretization approaches applicable to both time–steppers and GEVP solutions, although the present article will be devoted almost exclusively to the latter. As is known from classic linear instability analysis Mack (1984) accuracy is of prime concern also in global instability work. This need not translate to the necessity for high–order numerical methods for the spatial discretization of the LNSE operators, but such methods are increasingly more convenient to use as the Reynolds number increases, the structures to be resolved become increasingly tighter and the corresponding resolution requirements become more stringent. Nevertheless, successful global instability analyses have been reported in the literature, using both the low– and the high–order methods shown in this chart. To the best of the authors' knowledge, the first works featuring numerical methods shown in the lower case in figure 1 are discussed next.

In the context of methods of low formal order of accuracy, finite–difference methods were used by Crouch *et al.* Crouch et al. (2007) in a shock–capturing context and by Giannetti and Luchini Giannetti & Luchini (2007) in conjunction with an immersed–boundary approach. The respective methods dealt successfully with flow instability around a wing at realistic flight conditions and low–Reynolds number flow in the classic cylinder wake. Kuhlmann and co–workers (e.g. Albensoeder et al. (2001a;b)) and Sahin and Owens Sahin & Owens (2003) have used standard finite–volume methods in order to analyze the stability of lid–driven cavity flow Theofilis (AIAA-2000-1965). Marquet *et al.* Marquet et al. (2006) have employed low–order finite–element methods to the solution of the stability and control problems in an internal (S-shaped duct) flow, while González *et al.* González et al. (2007) have employed methods of the same class to the solution of global stability problems in both internal (rectangular duct and triangular cavity) and open (bluff–body wake) flows.

Turning to high–order methods, Henningson Henningson (1987) and Tatsumi and Yoshimura Tatsumi & Yoshimura (1990) were the first to introduce Fourier and Chebyshev (single–domain) spectral collocation methods, respectively, into inviscid and viscous global linear instability analysis. Spectral collocation has been the main workhorse of global instability research in the last decade; see Theofilis Theofilis (2011) for a review. De Vicente *et al.* de Vicente et al. (2006) and Robinet Robinet (2007) have discussed multidomain spectral collocation methodologies for the solution of incompressible (open cavity) and compressible (shock–induced laminar separation bubble) global flow stability problems, respectively. Barkley and Henderson Barkley & Henderson (1996) first employed Floquet theory and a structured spectral–element method to identify bifurcations in the wake of a circular cylinder, while Theofilis *et al.* Theofilis et al. (2002) were the first to introduce spectral/hp methods Karniadakis & Sherwin (2005) in order to address stability of flow in the wake of a NACA–0012 airfoil by solution of the BiGlobal eigenvalue problem. Abdessemed *et al.* Abdessemed et al. (2004; 2006) extended the spectral/hp methodology to the study of time–periodic flows in the wake of a low–pressure turbine. Finally, compact finite–difference methods have been introduced into the study of aeroacoustic and hydrodynamic global instability problems by Theofilis and Colonius Theofilis & Colonius (2003; 2004) and Bres and Colonius Bres & Colonius (2008), in the context of analysis of compressible laminar flow over an open cavity.

Short of describing in–depth the many successes of global instability theory, the main objective of the present article is to familiarize the reader with the concepts of this analysis methodology and present in detail techniques which the authors have employed in the course of their research in the past decade. The intention is not only to generate a self–contained manuscript, in which sufficient detail is presented for newcomers to the field to be able to construct their own solvers, but also to expose implementation aspects which may condition decisions on which method is to be chosen for the numerical solution of the eigenvalue problem. Section 2 presents separately the equations governing the incompressible and compressible limits, since the size of the associated problems makes inefficient the use of a single (compressible) code for the flow instability analysis at all Mach numbers. In addition, attention is paid to the adjoint eigenvalue problem, which underlies theoretically–founded flow control methodologies, and the the compressible Rayleigh equation, which may be used for computational aeroacoustics work. Section 3 discusses in–depth finite–element, spectral collocation (in both their single– and multi–domain flavor) and spectral/hp methods for the spatial discretization of the BiGlobal eigenvalue problem. A short section 4 presents the Arnoldi algorithm invariably used for the recovery of an arbitrarily–large window of eigenvalues, while a selection of results obtained by the authors is shown in section 5. A brief discussion in section 6 closes the presentation.

2. The linearized Navier-Stokes equations

The analysis of flow instability is based on the compressible equations of motion

$$\frac{\partial \rho}{\partial t} + \nabla \cdot (\rho \mathbf{u}) = 0, \tag{1}$$

$$\frac{\partial (\rho \mathbf{u})}{\partial t} + \nabla \cdot (\rho \mathbf{u}\mathbf{u}) = \frac{-1}{\gamma M^2} \nabla p + \frac{1}{Re} \nabla \cdot \boldsymbol{\text{œ}}, \tag{2}$$

$$\frac{\partial p}{\partial t} + \mathbf{u} \cdot \nabla p + \gamma p \nabla \cdot \mathbf{u} = \frac{\gamma}{RePr} \nabla \cdot (\kappa \nabla T) + \frac{\gamma(\gamma - 1) M^2}{Re} \Phi, \tag{3}$$

where,

$$\boldsymbol{\text{œ}} = \mu \left[(\nabla \mathbf{u} + \nabla \mathbf{u}^T) - \frac{2}{3} (\nabla \cdot \mathbf{u}) \, \mathbf{I} \right]$$

and

$$\Phi = \frac{1}{2} (\nabla \mathbf{u} + \nabla \mathbf{u}^T) : \boldsymbol{\text{œ}}$$

are the viscous stress tensor and the dissipation function, respectively, and Stokes' hypothesis is invoked. The equation of state of perfect gases,

$$p = \rho T,$$

valid up to hypersonic Mach numbers, is used in order to close this system of equations; under these conditions $\gamma = 7/5$ and $Pr = 0.72$ is taken to be a constant. In line with the analogous assumption of classic linear theory Mack (1984), the viscosity is assumed to be a function of temperature alone,

$$\mu = \mu(T).$$

Central to linear flow instability research is the concept of decomposition of any flow quantity into an $O(1)$ steady or time–periodic laminar *basic* flow upon which small–amplitude three–dimensional disturbances are permitted to develop. The most general framework in which a linear instability analysis can be performed is one in which three inhomogeneous spatial directions are resolved and time–periodic small–amplitude disturbances, *inhomogeneous* in all three directions, are superimposed upon the underlying steady or time-periodic $O(1)$ basic state. The related three-dimensional global *TriGlobal* instability Ansatz (named according to the dimensionality of the basic stateTheofilis (2003)) yields a three-dimensional eigenvalue problem in which all three spatial directions must be resolved simultaneously in a coupled manner. Though this most general Ansatz is consistent with the separability in the governing equations of time on the one hand and the three spatial directions on the other, the size of the resulting EVP is such that currently available computing hardware and algorithms permit its solution in a very limited range of Reynolds numbers, of $Re \approx O(10^2)$. A time–stepping approach for the TriGlobal EVP is discussed in another contribution to the present volume.

2.1 BiGlobal linear theory: the compressible two-dimensional linear EVP

In order to proceed in the context of global linear theory, the basic state is assumed independent of one spatial coordinate, say z, in a Cartesian framework. Flow quantities are then decomposed according to

$$\mathbf{q}(x,y,z,t) = \bar{\mathbf{q}}(x,y) + \varepsilon\, \tilde{\mathbf{q}}(x,y,z,t), \tag{4}$$

with $\bar{\mathbf{q}} = (\bar{u},\bar{v},\bar{w},\bar{T},\bar{p})^{\mathrm{T}}$ and $\tilde{\mathbf{q}} = (\tilde{u},\tilde{v},\tilde{w},\tilde{T},\tilde{p})^{\mathrm{T}}$ representing the steady *two-dimensional* basic flow and the unsteady *three-dimensional* infinitesimal perturbations, respectively, the latter being inhomogeneous in x and y and periodic in z. Note also that, unlike the incompressible case which will be discussed shortly, pressure is a predictive variable in, rather than a constraint of, the equations of motion. On substituting (4) into the governing equations (1-3), taking $\varepsilon \ll 1$ and linearizing about $\bar{\mathbf{q}}$, one may write

$$\tilde{\mathbf{q}}(x,y,z,t) = \hat{\mathbf{q}}(x,y)\, \mathrm{e}^{\mathrm{i}\,\Theta_{2\mathrm{D}}} + c.c., \tag{5}$$

with $\hat{\mathbf{q}} = (\hat{u},\hat{v},\hat{w},\hat{\theta},\hat{p})^{\mathrm{T}}$ representing the vector of *two–dimensional* complex amplitude functions of the infinitesimal three-dimensional perturbations, ω a complex eigenvalue and

$$\Theta_{2\mathrm{D}} = \beta z - \omega t \tag{6}$$

a complex phase function.

The linear disturbance equations of BiGlobal stability analysis are obtained at $O(\varepsilon)$ by substituting the decomposition (4-6) into the equations of motion, subtracting out the $O(1)$ basic flow terms and neglecting terms at $O(\varepsilon^2)$. In the present temporal framework, β is

taken to be a real wavenumber parameter describing an eigenmode in the $z-$direction, while the complex eigenvalue ω, and the associated eigenvectors $\hat{\mathbf{q}}$ are sought. The real part of the eigenvalue, $\omega_\mathrm{r} \equiv \Re\{\omega\}$, is related with the frequency of the global eigenmode while the imaginary part is its growth/damping rate; a positive value of $\omega_\mathrm{i} \equiv \Im\{\omega\}$ indicates exponential growth of the instability mode $\tilde{\mathbf{q}} = \hat{\mathbf{q}} \mathrm{e}^{\mathrm{i}\,\Theta_{2\mathrm{D}}}$ in time t while $\omega_\mathrm{i} < 0$ denotes decay of $\tilde{\mathbf{q}}$ in time. The system for the determination of the eigenvalue ω and the associated eigenfunctions $\hat{\mathbf{q}}$ in its most general form can be written as the complex nonsymmetric generalized EVP

$$\mathcal{L}\,\hat{\mathbf{q}} = \omega \mathcal{R}\,\hat{\mathbf{q}}, \tag{7}$$

or, more explicitly,

$$\begin{pmatrix} \mathcal{L}_{x\hat{u}} & \mathcal{L}_{x\hat{v}} & \mathcal{L}_{x\hat{w}} & \mathcal{L}_{x\hat{\theta}} & \mathcal{I}\mathcal{L}_{x\hat{p}} \\ \mathcal{L}_{y\hat{u}} & \mathcal{L}_{y\hat{v}} & \mathcal{L}_{y\hat{w}} & \mathcal{L}_{y\hat{\theta}} & \mathcal{I}\mathcal{L}_{y\hat{p}} \\ \mathcal{L}_{z\hat{u}} & \mathcal{L}_{z\hat{v}} & \mathcal{L}_{z\hat{w}} & \mathcal{L}_{z\hat{\theta}} & \mathcal{I}\mathcal{L}_{z\hat{p}} \\ \mathcal{L}_{e\hat{u}} & \mathcal{L}_{e\hat{v}} & \mathcal{L}_{e\hat{w}} & \mathcal{L}_{e\hat{\theta}} & \mathcal{I}\mathcal{L}_{e\hat{p}} \\ \mathcal{J}\mathcal{L}_{c\hat{u}} & \mathcal{J}\mathcal{L}_{c\hat{v}} & \mathcal{J}\mathcal{L}_{c\hat{w}} & \mathcal{J}\mathcal{L}_{c\hat{\theta}} & \mathcal{L}^G_{c\hat{p}} \end{pmatrix} \begin{pmatrix} \hat{u} \\ \hat{v} \\ \hat{w} \\ \hat{\theta} \\ \hat{p} \end{pmatrix} = \omega \begin{pmatrix} \mathcal{R}_{x\hat{u}} & 0 & 0 & 0 & 0 \\ 0 & \mathcal{R}_{y\hat{v}} & 0 & 0 & 0 \\ 0 & 0 & \mathcal{R}_{z\hat{w}} & 0 & 0 \\ 0 & 0 & 0 & 0 & \mathcal{I}\mathcal{R}_{e\hat{p}} \\ 0 & 0 & 0 & \mathcal{J}\mathcal{R}_{c\hat{\theta}} & \mathcal{R}^G_{c\hat{p}} \end{pmatrix} \begin{pmatrix} \hat{u} \\ \hat{v} \\ \hat{w} \\ \hat{\theta} \\ \hat{p} \end{pmatrix}, \tag{8}$$

subject to appropriate boundary conditions. Here the linearized equation of state

$$\hat{p} = \hat{\rho}/\bar{\rho} + \hat{\theta}/\bar{T}$$

has been used, viscosity and thermal conductivity of the medium have been taken as functions of temperature alone, resulting in

$$\hat{\mu} = \frac{d\bar{\mu}}{dT}\hat{\theta},\ \hat{\kappa} = \frac{d\bar{\kappa}}{dT}\hat{\theta}.$$

Moreover,

$$\mathcal{I} = I^G_{GL},\ \mathcal{J} = I^{GL}_G$$

are interpolation arrays transferring data from the Gauss–Lobatto to the Gauss and from the Gauss to the Gauss-Lobatto spectral collocation grids, respectively. Details on the spectral collocation spatial discretization will be provided in § 3.1. All submatrices of matrix $\mathcal{L}$ are defined on a two–dimensional Chebyshev Gauss-Lobatto (CGL) grid, except for $\mathcal{L}^G_{c\hat{p}}$ and $\mathcal{R}^G_{c\hat{p}}$, which are defined on a two–dimensional Chebyshev Gauss (CG) grid.

2.2 Classic linear theory: the one-dimensional compressible linear EVP

It is instructive at this point to compare the theory based on solution of (7) against results obtained by use of the established classic theory of linear instability of boundary- and shear-layer flows (cf. MackMack (1984), MalikMalik (1991)). The latter theory is based on the Ansatz

$$\mathbf{q}(x,y,z,t) = \bar{\mathbf{q}}(y) + \varepsilon\,\hat{\mathbf{q}}(y)\,\mathrm{e}^{\mathrm{i}\,\Theta_{1\mathrm{D}}} + c.c. \tag{9}$$

In (9) $\hat{\mathbf{q}}$ is the vector of *one–dimensional* complex amplitude functions of the infinitesimal perturbations and ω is in general complex. The phase function, $\Theta_{1\mathrm{D}}$, is

$$\Theta_{1\mathrm{D}} = \alpha x + \beta z - \omega t, \tag{10}$$

where α and β are wavenumber parameters in the spatial directions x and z, respectively, underlining the wave-like character of the linear perturbations in the context of the one-dimensional EVP.
Substitution of the decomposition (9-10) into the governing equations (1-3) linearization and consideration of terms at $O(\varepsilon)$ results in the eigenvalue problem governing linear stability of boundary- and shear-layer flows; the same system results directly from (7) if one makes the following ("parallel flow") assumptions:

- $\partial\bar{q}/\partial x \equiv 0$, $\partial\bar{q}/\partial x \equiv 0$
  (basic flow independent of x),
  i.e. $\partial\hat{q}/\partial x \equiv \mathrm{i}\,\alpha\,\hat{q}$, $\partial\hat{q}/\partial z \equiv \mathrm{i}\,\beta\,\hat{q}$
  (harmonic expansion of disturbances in x and z),
- $\bar{v} \equiv 0$, and
- $\bar{p} \equiv cnst.$,

then (7) takes the form of the system of equations governing linear stability of viscous compressible boundary- and shear-layer flows (cf. eqns. (8.9) of Mack Mack (1984)). None of these approximations are necessary in the context of BiGlobal theory, but invoking the parallel flow assumption in the latter context provides direct means for comparisons between the present (relatively) novel and the established methodologies. Such comparisons have been performed, e.g. by Theofilis and Colonius Theofilis & Colonius (2004). It should be noted that the crucial difference between the two–dimensional eigenvalue problem (7) and the limiting case of the one–dimensional EVP is that the eigenvector $\hat{q}$ in (7) comprises *two–dimensional* amplitude functions, while those in the limiting parallel–flow case are *one–dimensional*. Further, while $\bar{p}(y) = cnst.$ in taken to be a constant in one-dimensional basic states satisfying (9), $\bar{p}(x,y)$ appearing in (7) is, in general, a known function of the two resolved spatial coordinates.

2.3 The compressible BiGlobal Rayleigh equation

Linearizing the viscous compressible equations of motion neglecting the viscous terms in (8) and introducing the elliptic confocal coordinate system Morse & Feshbach (1953) for reasons which will become apparent later leads to the generalized Rayleigh equation on this coordinate system,

$$\hat{p}_{\xi\xi} + \hat{p}_{\eta\eta} - h^2\beta^2\hat{p} + \frac{j_1^2+j_2^2}{h^2}\left[\left(\frac{\bar{p}_\xi}{\gamma\bar{p}} - \frac{\bar{\rho}_\xi}{\bar{\rho}}\right) - \frac{2\beta\bar{w}_\xi}{(\beta\bar{w}-\omega)}\right]\hat{p}_\xi + \frac{j_1^2+j_2^2}{h^2}\left[\left(\frac{\bar{p}_\eta}{\gamma\bar{p}} - \frac{\bar{\rho}_\eta}{\bar{\rho}}\right) - \frac{2\beta\bar{w}_\eta}{(\beta\bar{w}-\omega)}\right]\hat{p}_\eta + \left[\frac{\bar{\rho}\,(\beta\bar{w}-\omega)^2}{\gamma\bar{p}}\right]\hat{p} = 0. \tag{11}$$

Since the metrics of the elliptic confocal coordinate system satisfy $j_1^2 + j_2^2 = h^2$, one finally has to solve

$$\mathcal{M}\hat{p} + \left[\left(\frac{\bar{p}_{\xi}}{\gamma\bar{p}} - \frac{\bar{\rho}_{\xi}}{\bar{\rho}}\right) - \frac{2\beta\bar{w}_{\xi}}{(\beta\bar{w}-\omega)}\right]\hat{p}_{\xi} + \left[\left(\frac{\bar{p}_{\eta}}{\gamma\bar{p}} - \frac{\bar{\rho}_{\eta}}{\bar{\rho}}\right) - \frac{2\beta\bar{w}_{\eta}}{(\beta\bar{w}-\omega)}\right]\hat{p}_{\eta} + \left[\frac{\bar{\rho}\,(\beta\bar{w}-\omega)^2}{\gamma\bar{p}}\right]\hat{p} = 0. \tag{12}$$

where the linear operator $\mathcal{M} \equiv \partial_{\xi\xi} + \partial_{\eta\eta} - h^2\beta^2$. In a manner analogous with classic one-dimensional linear theory Mack (1984); Malik (1991), (12) may be solved either iteratively or by direct means. In view of the lack of any prior physical insight into global linear disturbances in the application at hand, a direct method is preferable on account of the access to the full eigenvalue spectrum that it provides. Either the temporal or the spatial form of the eigenvalue problem may be solved at the same level of numerical effort using a direct method since, in both cases, a cubic eigenvalue problem must be solved. In its temporal form, the temporal global inviscid instability problem reads

$$T_1\,\hat{p}_{\xi\xi} + T_2\,\hat{p}_{\eta\eta} + T_3\,\hat{p}_{\xi} + T_4\,\hat{p}_{\eta} + T_5\,\hat{p} = \omega\left(T_6\,\hat{p}_{\xi\xi} + T_7\,\hat{p}_{\eta\eta} + T_8\,\hat{p}_{\xi} + T_9\,\hat{p}_{\eta} + T_{10}\,\hat{p}\right) + \omega^2\,T_{11}\,\hat{p} + \omega^3\,T_{12}\,\hat{p} \tag{13}$$

while the spatial generalized Rayleigh equation on the elliptic confocal coordinate system is

$$S_1\,\hat{p}_{\xi\xi} + S_2\,\hat{p}_{\eta\eta} + S_3\,\hat{p}_{\xi} + S_4\,\hat{p}_{\eta} + S_5\,\hat{p} = \beta\left(S_6\,\hat{p}_{\xi\xi} + S_7\,\hat{p}_{\eta\eta} + S_8\,\hat{p}_{\xi} + S_9\,\hat{p}_{\eta} + S_{10}\,\hat{p}\right) + \beta^2\,S_{11}\,\hat{p} + \beta^3\,S_{12}\,\hat{p}. \tag{14}$$

In the incompressible limit, equation (11) reduces to that solved by Henningson Henningson (1987), while in the absence of flow (and its derivatives) altogether, (11) simplifies in the classic two-dimensional Helmholtz problem

$$\left(\partial_{\xi\xi} + \partial_{\eta\eta} + \kappa^2\right)\hat{p} = 0, \tag{15}$$

which has been recently employed extensively to the solution of resonance problems Hein et al. (2007); Koch (2007).

2.4 The incompressible limit

Since most global instability analysis work performed to-date has been in an incompressible flow context, this limit will now be described in a little more detail. The equations governing incompressible flows may be directly deduced from (1-3) and are written in

primitive-variables formulation

$$\frac{\partial u_i}{\partial t} + u_j \frac{\partial u_i}{\partial x_j} = -\frac{\partial p}{\partial x_i} + \frac{1}{Re} \frac{\partial^2 u_i}{\partial x_j^2} \qquad \text{in} \qquad \Omega, \tag{16}$$

$$\frac{\partial u_i}{\partial x_i} = 0 \qquad \text{in} \qquad \Omega. \tag{17}$$

Here Ω is the computational domain, u_i represents the velocity field, p is the pressure field, t is the time and x_i represent the spatial coordinates. This domain is limited by a boundary Γ where different boundary conditions can be imposed depending on the problem and the numerical dicretization. The primitive variable formulation is preferred over the alternative velocity-vorticity form, simply because the resulting system comprises four- as opposed to six equations which need to be solved in a coupled manner.

The two-dimensional equations of motion are solved in the laminar regime at appropriate Re regions, in order to compute steady real basic flows $(\bar{u}_i, \bar{p})$ whose stability will subsequently be investigated. The basic flow equations read

$$\frac{\partial \bar{u}_i}{\partial t} + \bar{u}_j \frac{\partial \bar{u}_i}{\partial x_j} = -\frac{\partial \bar{p}}{\partial x_i} + \frac{1}{Re} \frac{\partial^2 \bar{u}_i}{\partial x_j^2} \qquad \text{in} \qquad \Omega, \tag{18}$$

$$\frac{\partial \bar{u}_i}{\partial x_i} = 0 \qquad \text{in} \qquad \Omega \tag{19}$$

The steady laminar basic flow is obtained by time-integration of the system (18-19) starting from rest until the steady state is obtained. The convergence in time of the steady basic flow must be $O(10^{-12})$ to make it adequate for the linear analysis. In case of unsteady laminar or turbulent flows, one may analyze time-averaged mean flows. Finally, in the particular case of addressing laminar flow over a symmetric body, steady flows can be obtained by forcing a symmetry condition along the line of geometric symmetry.

The basic flow is perturbed by small-amplitude velocity u_i^* and kinematic pressure p^* perturbations, as follows

$$u_i = \bar{u}_i + \varepsilon u_i^* + c.c. \qquad p = \bar{p} + \varepsilon p^* + c.c., \tag{20}$$

where $\varepsilon \ll 1$ and $c.c.$ denotes conjugate of the complex quantities (u_i^*, p^*). Substituting into equations (16-17), subtracting the basic flow equations (18-19), and linearizing, the incompressible Linearized Navier-Stokes Equations (LNSE) for the perturbation quantities are obtained

$$\frac{\partial u_i^*}{\partial t} + \bar{u}_j \frac{\partial u_i^*}{\partial x_j} + u_j^* \frac{\partial \bar{u}_i}{\partial x_j} = -\frac{\partial p^*}{\partial x_i} + \frac{1}{Re} \frac{\partial^2 u_i^*}{\partial x_j^2}, \tag{21}$$

$$\frac{\partial u_i^*}{\partial x_i} = 0. \tag{22}$$

2.5 Time-marching

The initial condition for (21-22) must be inhomogeneous in order for a non-trivial solution to be obtained. In view of the homogeneity along one spatial direction, $x_3 \equiv z$, the most general form assumed by the small amplitude perturbations satisfies the following Ansatz

$$u_i^* = \hat{u}_i(x, y, t)e^{i\beta z} \tag{23}$$

$$p^* = \hat{p}(x, y, t)e^{i\beta z}, \tag{24}$$

where $i = \sqrt{-1}$, β is a wavenumber parameter, related with a periodicity length L_z along the homogeneous direction through $L_z = 2\pi/\beta$, $(\hat{u}_i, \hat{p})$ are the complex amplitude functions of the linear perturbations and *c.c.* denotes complex conjugates, introduced so that the LHS of equations (23-24) be real. Note that the amplitude functions may, at this stage, be arbitrary functions of time.

Substituting (23) and (24) into the equations (21) and (22), the equations may be reformulated as

$$\frac{\partial \hat{u}_1}{\partial t} + \bar{u}_j \frac{\partial \hat{u}_1}{\partial x_j} + \hat{u}_j \frac{\partial \bar{u}_1}{\partial x_j} = -\frac{\partial \hat{p}}{\partial x} + \frac{1}{Re}\left(\frac{\partial^2}{\partial x_j^2} - \beta^2\right)\hat{u}_1, \tag{25}$$

$$\frac{\partial \hat{u}_2}{\partial t} + \bar{u}_j \frac{\partial \hat{u}_2}{\partial x_j} + \hat{u}_j \frac{\partial \bar{u}_2}{\partial x_j} = -\frac{\partial \hat{p}}{\partial y} + \frac{1}{Re}\left(\frac{\partial^2}{\partial x_j^2} - \beta^2\right)\hat{u}_2, \tag{26}$$

$$\frac{\partial \hat{u}_3}{\partial t} + \bar{u}_j \frac{\partial \hat{u}_3}{\partial x_j} + \hat{u}_j \frac{\partial \bar{u}_3}{\partial x_j} = -i\beta\hat{p} + \frac{1}{Re}\left(\frac{\partial^2}{\partial x_j^2} - \beta^2\right)\hat{u}_3, \tag{27}$$

$$\frac{\partial \hat{u}_1}{\partial x} + \frac{\partial i\hat{u}_2}{\partial y} + i\beta\hat{u}_3 = 0. \tag{28}$$

This system may be integrated along time by numerical methods appropriate for the spatial discretization scheme utilized. The result of the time-integration at $t \to \infty$ is the leading eigenmode of the steady basic flow. In this respect, time-integration of the linearized disturbance equations is a form of power iteration for the leading eigenvalue of the system. Alternative, more sophisticated, time-integration approaches, well described by Karniadakis and Sherwin Karniadakis & Sherwin (2005) are also available for the recovery of both the leading and a relatively small number of additional eigenvalues. The key advantage of time-marching methods, over explicit formation of the matrix which describes linear instability, is that the matrix need never be formed. This enables the study of global linear stability problems on (relatively) small-main-memory machines at the expense of (relatively) long–time integrations. To–date this is the only viable approach to perform TriGlobal instability analysis. A potential pitfall of the time-integration approach is that results are sensitive to the quality of spatial integration of the linearized equations, such that this approach should preferably be used in conjunction with high-order spatial discretization methods; see Karniadakis & Sherwin (2005) for a discussion. The subsequent discussion will be exclusively focused on approaches in which the matrix is formed.

2.6 Matrix formation – the incompressible direct and adjoint BiGlobal EVPs

Starting from the (direct) LNSE (21-22) and assuming modal perturbations and homogeneity in the spanwise spatial direction, z, eigenmodes are introduced into the linearized direct Navier-Stokes and continuity equations according to

$$(\mathbf{q}^*, p^*) = (\hat{\mathbf{q}}(x,y), \hat{p}(x,y))\mathrm{e}^{+\mathrm{i}\,(\beta z - \omega t)}, \tag{29}$$

where $\mathbf{q}^* = (u^*, v^*, w^*)^{\mathrm{T}}$ and p^* are, respectively, the vector of amplitude functions of linear velocity and pressure perturbations, superimposed upon the steady two-dimensional, two-($\bar{w} \equiv 0$) or three-component, $\bar{\mathbf{q}} = (\bar{u}, \bar{v}, \bar{w})^T$, steady basic states. The spanwise wavenumber β is associated with the spanwise periodicity length, L_z, through $L_z = 2\pi/L_z$. Substitution of (29) into (21-22) results in the complex *direct* BiGlobal eigenvalue problem Theofilis (2003)

$$\hat{u}_x + \hat{v}_y + i\beta\hat{w} = 0, \tag{30}$$

$$(\mathcal{L} - \bar{u}_x + \mathrm{i}\,\omega)\,\hat{u} - \bar{u}_y\hat{v} - \hat{p}_x = 0, \tag{31}$$

$$-\bar{v}_x\hat{u} + \left(\mathcal{L} - \bar{v}_y + \mathrm{i}\,\omega\right)\hat{v} - \hat{p}_y = 0, \tag{32}$$

$$-\bar{w}_x\hat{u} - \bar{w}_y\hat{v} + (\mathcal{L} + i\omega)\,\hat{w} - i\beta\hat{p} = 0, \tag{33}$$

where

$$\mathcal{L} = \frac{1}{Re}\left(\frac{\partial^2}{\partial x^2} + \frac{\partial^2}{\partial y^2} - \beta^2\right) - \bar{u}\frac{\partial}{\partial x} - \bar{v}\frac{\partial}{\partial y} - i\beta\bar{w}. \tag{34}$$

The concept of the adjoint eigenvalue problem has been introduced in the context of receptivity and flow control respectively by Zhigulev and Tumin Zhigulev & Tumin (1987) and Hill Hill (1992). The derivation of the complex BiGlobal eigenvalue problem governing adjoint perturbations is constructed using the Euler-Lagrange identity Bewley (2001); Dobrinsky & Collis (2000); Giannetti & Luchini (2007); Morse & Feshbach (1953); Pralits & Hanifi (2003),

$$\begin{aligned}\left[\left(\frac{\partial\hat{\mathbf{q}}^*}{\partial t} + \mathcal{N}\hat{\mathbf{q}}^* + \nabla\hat{p}^*\right)\cdot\tilde{\mathbf{q}}^* + \nabla\cdot\hat{\mathbf{q}}^*\tilde{p}^*\right] + \\ \left[\hat{\mathbf{q}}^*\cdot\left(\frac{\partial\tilde{\mathbf{q}}^*}{\partial t} + \mathcal{N}^\dagger\tilde{\mathbf{q}}^* + \nabla\tilde{p}^*\right) + \hat{p}^*\nabla\cdot\tilde{\mathbf{q}}^*\right] = \\ \frac{\partial}{\partial t}(\hat{\mathbf{q}}^*\cdot\tilde{\mathbf{q}}^*) + \nabla\cdot j(\hat{\mathbf{q}}^*, \tilde{\mathbf{q}}^*),\end{aligned} \tag{35}$$

as applied to the linearized incompressible Navier-Stokes and continuity equations. Here the operator $\mathcal{N}^\dagger(\bar{\mathbf{q}})$ results from linearization of the convective and viscous terms in the direct and adjoint Navier-Stokes equations and is explicitly stated elsewhere (e.g. Dobrinsky & Collis (2000)). The quantities $\tilde{\mathbf{q}}^* = (\tilde{u}^*, \tilde{v}^*, \tilde{w}^*)^{\mathrm{T}}$ and $\tilde{p}^*$ denote adjoint disturbance velocity components and adjoint disturbance pressure, and $j(\hat{\mathbf{q}}^*, \tilde{\mathbf{q}}^*)$ is the bilinear concomitant. Vanishing of the RHS term in the Euler-Lagrange identity (35) defines the adjoint linearized incompressible Navier-Stokes and continuity equations

$$\frac{\partial\tilde{\mathbf{q}}^*}{\partial t} + \mathcal{N}^\dagger\tilde{\mathbf{q}}^* + \nabla\tilde{p}^* = 0, \tag{36}$$

$$\nabla\cdot\tilde{\mathbf{q}}^* = 0, \tag{37}$$

Assuming modal perturbations and homogeneity in the spanwise spatial direction, z, eigenmodes are introduced into (36-37) according to

$$(\tilde{\mathbf{q}}^*, \tilde{p}^*) = (\tilde{\mathbf{q}}(x,y), \tilde{p}(x,y))\mathrm{e}^{-\mathrm{i}\,(\beta z - \omega t)}. \tag{38}$$

Note the opposite signs of the spatial direction z and time in (29) and (38), denoting propagation of $\tilde{\mathbf{q}}^*$ in the opposite directions compared with the respective one for $\hat{\mathbf{q}}^*$. Substitution of (38) into the adjoint linearized Navier-Stokes equations (36-37) results in the complex *adjoint* BiGlobal EVP

$$\tilde{u}_x + \tilde{v}_y - \mathrm{i}\,\beta\tilde{w} = 0, \tag{39}$$

$$\left(\mathcal{L}^\dagger - \bar{u}_x + \mathrm{i}\,\omega\right)\tilde{u} - \bar{v}_x\tilde{v} - \bar{w}_x\tilde{w} - \tilde{p}_x = 0, \tag{40}$$

$$-\bar{u}_y\tilde{u} + \left(\mathcal{L}^\dagger - \bar{v}_y + \mathrm{i}\,\omega\right)\tilde{v} - \bar{w}_y\tilde{w} - \tilde{p}_y = 0, \tag{41}$$

$$\left(\mathcal{L}^\dagger + \mathrm{i}\,\omega\right)\tilde{w} + \mathrm{i}\,\beta\tilde{p} = 0, \tag{42}$$

where

$$\mathcal{L}^\dagger = \frac{1}{Re}\left(\frac{\partial^2}{\partial x^2} + \frac{\partial^2}{\partial y^2} - \beta^2\right) + \bar{u}\frac{\partial}{\partial x} + \bar{v}\frac{\partial}{\partial y} - \mathrm{i}\,\beta\bar{w}. \tag{43}$$

Note also that, in the particular case of two–component two–dimensional basic states, i.e. $(\bar{u} \neq 0, \bar{v} \neq 0, \bar{w} \equiv 0)^{\mathrm{T}}$ such as encountered, f.e. in the lid–driven cavity Theofilis (AIAA-2000-1965) and the laminar separation bubble Theofilis et al. (2000), both the direct and adjoint EVP may be reformulated as *real EVPs* Theofilis (2003); Theofilis, Duck & Owen (2004), thus saving half of the otherwise necessary memory requirements for the coupled numerical solution of the EVPs (30-33) and (39-42).

Boundary conditions for the partial-derivative adjoint EVP in the case of a closed system are particularly simple, requiring vanishing of adjoint perturbations at solid walls, much like the case of their direct counterparts. In open systems containing boundary layers, adjoint boundary conditions may be devised following the general procedure of expanding the bilinear concomitant in order to capture traveling disturbances Dobrinsky & Collis (2000). When the focus is on global modes concentrated in certain regions of the flow, as the case is, for example, for the global mode of laminar separation bubble (Theofilis (2000); Theofilis et al. (2000)) the following procedure may be followed. For the direct problem, homogeneous Dirichlet boundary conditions are used at the inflow, $x = x_{IN}$, wall, $y = 0$, and far-field, $y = y_\infty$, boundaries, alongside linear extrapolation at the outflow boundary $x = x_{OUT}$. Consistently, homogeneous Dirichlet boundary conditions at $y = 0$, $y = y_\infty$ and $x = x_{OUT}$, alongside linear extrapolation from the interior of the computational domain at $x = x_{IN}$, are used in order to close the adjoint EVP.

Once the eigenvalue problem has been stated, the objective becomes its numerical solution in any of its compressible viscous (8), inviscid (11), or incompressible (30-33) direct or adjoint forms. Any of these eigenvalue problems is a system of coupled partial-differential equations for the determination of the eigenvalues, ω, and the associated sets of amplitude functions, $\hat{\mathbf{q}}$. Intuitively one sees that, when the matrix is formed, resolution/memory requirements will be the main concern of any numerical solution approach and this is indeed the case in all

but the smallest (and least interesting) Reynolds number values. The following discussion is devoted to this point and is divided in two parts, one devoted to the spatial discretization of the PDE-based EVP and one dealing with the subspace iteration method used for the determination of the eigenvalue.

3. Numerical discretization – weighted residual methods

The approximation of a function u as an expansion in terms of a sequence of orthogonal functions, is the starting point of many numerical methods of approximation. Spectral methods belong to the general class of weighted residuals methods (WRM). These methods assume that a solution of a differential equation can be approximated in terms of a truncated series expansion, such that the difference between the exact and approximated solution (residual), is minimized.

Depending on the set of base (trial) functions used in the expansion and the way the error is forced to be zero several methods are defined. But before starting with the classification of the different types of WRM it is instructive to present a brief introduction to vector spaces.

Define the set,

$$\mathcal{L}^2_w(I) = \{v : I \to \mathcal{R} |\ v \text{ is measurable and } \| v \|_{o,w} < \infty\}$$

where $w(x)$ denotes a weight function, i.e., a continuous, strictly positive and integrable function over the interval $I = (-1, 1)$ and

$$\| v \|_w = \left(\int_{-1}^{1} |v(x)|^2 w(x) dx \right)^{1/2}$$

is the norm induced by the scalar product

$$(u, v)_w = \int_{-1}^{1} u(x) v(x) w(x) dx$$

Let $\{\varphi_n\}_{n \geq 0} \in \mathcal{L}^2_w(I)$ denote a system of algebraic polynomials, which are mutually orthogonal under the scalar product defined before.

$$(\varphi_n, \varphi_m)_w = 0 \text{ whenever } m \neq n$$

Using the Weierstrass approximation theorem every continuous function included in $\mathcal{L}^2_w(-1, 1)$ can be uniformly approximated as closely as desired by a polynomial expansion, i.e. for any function u the following expansion holds

$$u(x) = \sum_{k=0}^{\infty} \hat{u}_k \varphi_k(x) \text{ with } \hat{u}_k = \frac{(u, \varphi_k)_w}{\| \varphi_k \|^2_{0,w}} \tag{44}$$

The $\hat{u}_k$ are the expansion coefficients associated with the basis $\{\varphi_n\}$, defined as

$$\hat{u}_k = \frac{1}{\| \varphi_k \|^2_{0,w}} \int_{-1}^{1} u(x) \varphi_k(x) w(x) dx \tag{45}$$

Consider now the truncated series of order N

$$u_N(x) = \sum_{k=0}^{N} \hat{u}_k \varphi_k(x)$$

$u_N(x)$ is the orthogonal projection of u upon the span of $\{\varphi_n\}$.
Due to the completeness of the system $\{\varphi_n\}$, the truncated series converges in the sense of $\forall u \in \mathcal{L}^2_w(I)$

$$\| u - u_N \|_w \to 0 \text{ as } N \to \infty$$

Now the residual could be defined as

$$\mathcal{R}_N(x) = u - u_N$$

In the weighted residuals methods the goal of annulling $\mathcal{R}_N$ is reached in an approximate sense by setting to zero the scalar product

$$(\mathcal{R}_N, \phi_i)_{\hat{w}} = \int_{-1}^{1} \mathcal{R}_N \phi_i(x) \hat{w}(x) dx$$

where ϕ_i are test functions and $\hat{w}$ is the weight associated with the trial function.

A first and main classification of the different WRM is done depending on the choice of the trial functions φ_i. Finite Difference and Finite Element methods use overlapping local polynomials as base functions.
In Spectral Methods, however, the trial functions are global functions, typically tensor products of the eigenfunctions of singular Sturm-Liouville problems. Some well–known examples of these functions are: Fourier trigonometric functions for periodic– and Chebyshev or Legendre polynomials for nonperiodic problems.

Focusing on the Spectral Methods and attending to the residual, a second distinction could be:

- Galerkin approach: This method is characterized by the choice $\phi_i = \varphi_i$ and $\hat{w} = w$. Therefore, the residual

  $$\mathcal{R}_N(x) = u - u_N = u - \sum_{k=0}^{N} \hat{u}_k \varphi_k(x)$$

  is forced to zero in the mean according to

  $$(\mathcal{R}_N, \varphi_i)_w = \int_{-1}^{1} \left(u - \sum_{k=0}^{N} \hat{u}_k \varphi_k \right) \varphi_i w dx = 0 \quad i = 0, ..., N.$$

These $N+1$ Galerkin equations determine the coefficients $\hat{u}_k$ of the expansion.

- Collocation approach: The test functions are Dirac delta-functions $\phi_i = \delta(x - x_i)$ and $\hat{w} = 1$.
  The collocation points x_i, are selected as will be discussed later.Now, the residual

$$\mathcal{R}_N(x) = u - u_N = u - \sum_{k=0}^{N} \hat{u}_k \varphi_k(x)$$

  is made equal zero at the $N+1$ collocation points, $u(x_i) - u_N(x_i)$, hence,

$$\sum_{k=0}^{N} \hat{u}_k \varphi_k(x) = u(x_i)$$

  This gives an algebraic system to determine the $N+1$ coefficients $\hat{u}_k$.

- Tau approach: It is a modification of the Galerkin approach allowing the use of trial functions not satisfying the boundary conditions; it will not be discussed in the present context.

3.1 Spectral collocation methods

In the general framework of Spectral Methods the approximation of a function u is done in terms of global polynomials. Appropriate choices for non-periodic functions are Chebyshev or Legendre polynomials, while periodic problems may be treated using the Fourier basis. The exposition that follows will be made on the basis of the Chebyshev expansion only.

3.1.1 Collocation approximation

The Chebyshev polynomials of the first kind $T_k(x)$ are the eigenfunctions of the singular Sturm-Liouville problem

$$\begin{cases} -(pu')' + qu = \lambda w u & \text{in the interval } (1,-1) \\ \text{plus boundary conditions for } u \end{cases}$$

where $p(x) = (1-x^2)^{1/2}$, $q(x) = 0$ and $w(x) = (1-x^2)^{-1/2}$. The problem is reduced to

$$(\sqrt{1-x^2}T_k'(x))' + \frac{k^2}{\sqrt{1-x^2}}T_k(x) = 0$$

For $x \in [-1,1]$ an important characterization is given by

$$T_k(x) = \cos k\theta \quad \text{with } \theta = \arccos x$$

One of the main features of the Chebyshev polynomials is the orthogonality relationship, Chebyshev family is orthogonal in the Hilbert space $\mathcal{L}^2_w[-1,1]$, with the weight $w(x) = (1-x^2)^{-1/2}$.

$$(T_k, T_l)_w = \int_{-1}^{1} T_k(x)T_l(x)w(x)dx = \frac{\pi}{2}c_k\delta_{k,l}$$

where $\delta_{k,l}$ is the Kronecker delta and c_k is defined as:

$$c_k = \begin{cases} 2 & \text{if } k = 0 \\ 1 & \text{if } k \geq 1 \end{cases}$$

The spectral Chebyshev representation of any function $u(x)$ defined for $x \in [-1,1]$ is its orthogonal projection on the space of polynomials of degree $\leq N$:

$$u_N(x) = \sum_{k=0}^{N} \hat{u}_k T_k(x)$$

in the collocation method the expansion coefficients are calculated so the residual is setting to zero at the collocation points. The choice of such points is not arbitrary, depends on the quadrature formulas for integration used and the characteristics of the problem tackled:

Chebyshev-Gauss points,

$$x_i = \cos\frac{(2i+1)\pi}{2N+2}; \quad i = 0,..,N \tag{46}$$

are the roots of the Chebyshev polynomial T_{N+1}, and are related to the Gauss integration in $(-1,1)$.

Chebyshev-Gauss-Lobatto points

$$x_i = \cos\frac{i\pi}{N} \quad i = 0,..,N \tag{47}$$

are the points where T_N reaches its extremal values. Gauss-Lobatto nodes are related to the Gauss-Lobatto integration and include the end points ± 1, useful if there is a requirement of imposing boundary conditions.

As mentioned the technique consists of setting to zero the residual $R_N = u - u_N$ at the collocation points x_i, $i = 0,..,N$, so

$$\sum_{k=0}^{N} \hat{u}_k T_k(x_i) = u(x_i), i = 0,...N.$$

This gives an algebraic system to determine the $N+1$ coefficients $\hat{u}_k, k = 0,...,N$. The existence of a solution implies that $detT_k(x_i) \neq 0$.
As a matter of fact the expression for the coefficients can be found without solving the system, this is done using the discrete orthogonality property of the basis functions. From the Gauss quadrature formula,

$$\int_{-1}^{1} pwdx \cong \frac{\pi}{N} \sum_{i=0}^{N} \frac{p(x_i)}{\hat{c}_i}$$

where

$$\hat{c}_i = \begin{cases} 2 & \text{if } i = 0, N \\ 1 & \text{if } i = 1, ..., N-1 \end{cases}$$

This relation is exact when $p(x)$ is a polynomial of degree less than $2N$, so using the Chebyshev-Gauss-Lobatto collocation points and since $T_k T_l$ is a polynomial of degree at most $2N-1$ the discrete orthogonality property is deduced:

$$\int_{-1}^{1} T_k(x) T_l(x) w(x) dx = \frac{\pi}{N} \sum_{i=0}^{N} \frac{1}{\hat{c}_i} T_k(x_i) T_l(x_i)$$

therefore

$$\sum_{i=0}^{N} \frac{1}{\hat{c}_i} T_k(x_i) T_l(x_i) = \frac{\hat{c}_k}{2} N \delta_{k,l}$$

Now, multiplying each side of (the equation for residual), by $T_l(x_i)/\hat{c}_i$, summing from $i = 0$ to $i = N$, and using the discrete orthogonality relation, the next expression for the collocation coefficients is obtained:

$$\hat{u}_k = \frac{2}{\hat{c}_k N} \sum_{-1}^{1} \frac{1}{\hat{c}_i} u(x_i) T_k(x_i) \text{ , } k = 0, ..., N. \tag{48}$$

It must be noted that such expression is nothing but the numerical approximation of the integral form. The grid values $u(x_i)$ and the expansion coefficients $\hat{u_k}$ are related by truncated discrete Fourier series in cosine, so it is possible to use the Fast Fourier Transform (FFT) to connect the physical space to the spectral space.

From other point of view the expression for the approximation of a function using the collocation technique at the Chebyshev-Gauss-Lobatto points,

$$u_N(x) = \sum_{k=0}^{N} \hat{u}_k T_k(x)$$

could be seen as the Lagrange interpolation polynomial of degree N based on the set x_i. Hence it can be written in the form

$$u_N(x) = \sum_{k=0}^{N} h_k u(x_j) \tag{49}$$

where the Lagrange functions $h_j \in \mathcal{P}_{\mathcal{N}}$ are such that $h_j(x_k) = \delta_{jk}$ and are defined by

$$h_j(x) = \frac{(-1)^{j+1}(1-x^2)T_N^{'}(x)}{\hat{c}_j N^2(x-x_j)}$$

This expression for the approximation does not involve the spectral coefficients, the unknowns are the grid values what makes it useful for expressing the derivatives at any collocation point in terms of the grid values of the function.

$$(\partial_N u)(x_j) = \sum_{k=0}^{N} h_k^{'}(x_j)u(x_k),\ j = 0, ..., N. \tag{50}$$

The matrix $(D_N)_{ij} = h_j^{'}(x_i)$ is named Chebyshev pseudo-spectral matrix and its entries can be computed explicitly,

$$(D_N)_{ij} = \begin{cases} \frac{\hat{c}_i}{\hat{c}_j}\frac{(-1)^{i+j}}{(x_i-x_j)} & \text{if } 0 \le i,j \le N, i \ne j \\ -\frac{x_i}{2(1-x_i^2)} & \text{if } 1 \le i = j \le N-, i \ne j \\ \frac{2N^2+1}{6} & \text{if } 0 = i = j \\ -\frac{2N^2+1}{6} & \text{if } i = j = N \end{cases} \tag{51}$$

In vector form the derivatives may be expressed as

$$U' = \mathcal{D}U \approx \begin{pmatrix} d_{0,0} & d_{0,1} & \dots & d_{0,N} \\ d_{1,0} & d_{1,1} & \dots & d_{1,N} \\ & & \ddots & \\ d_{N,0} & d_{N,1} & \dots & d_{N,N} \end{pmatrix} \begin{pmatrix} U_0 \\ U_1 \\ \\ U_N \end{pmatrix} = (U_0', U_1', \dots, U_N') \tag{52}$$

Second derivatives may be computed explicitly, although it is useful to recall that $U'' = \mathcal{D}(\mathcal{D}U) = \mathcal{D}^2 U$

3.1.2 Mappings

Expansion in Chebyshev polynomials of functions defined on other finite intervals from $[-1,1]$ are required not only owing to geometric demands but also when the function has regions of rapid change, boundary layers, singularities and so on. Mappings can be useful in improving the accuracy of a Chebyshev expansion.

But not any choice of the collocation points x_i is appropriate, the polynomial approximation on them does not necessarily converge when $N \to \infty$.

If $x \in [-1,1]$ the coordinate transformation $y = f(x)$ must meet some requirements. It must be one-to-one, easy to invert and at least C^1. So, let

$$A = [a,b] \text{ with } y \in A$$

the physical space, and f the mapping in the form

$$y = f(x)$$

The approximation of a function u in $A = [a,b]$ can be easily done assuming $u_N(y) = u_N(f(x)) = v_N(x)$. The Chebyshev expansion:

$$u_N(y) = \sum_{k=0}^{N} \hat{v}_k T_k(x)$$

Now the goal is to represent the derivative of u in terms of its values in y_N. From elementary calculus

$$\frac{d}{dx} = \frac{d}{dy}\frac{dy}{dx} = \frac{d}{dy}\frac{df(x)}{dx} \text{ so}$$

$$\frac{d}{dy} = \frac{1}{f'(x)}\frac{d}{dx}$$

where $f' = dy/dx$.

In vector form and using Chebyshev pseudo-spectral matrix the derivatives of a function $u(y)$ with $y \in A$ may be expressed as:

$$U'_y = D_y \, \mathcal{D}U(x)$$

where $D_y = dx/dy$.
The expression for second derivatives of u incorporating the metrics of the transformation can be computed explicitly:

$$\frac{d^2}{dy^2} = \frac{d}{dy}\left(\frac{d}{dx}\right)\frac{dx}{dy} + \frac{d}{dx}\left(\frac{d^2x}{dy^2}\right) =$$

$$= \frac{d^2}{dx^2}\left(\frac{dx}{dy}\right)^2 + \frac{d}{dx}\left(\frac{d^2x}{dy^2}\right)$$

3.1.3 Stretching

Frequently the situation arises where fine flow structures in boundary layers forming on complex bodies must be adequately resolved. While the natural distribution of the Chebyshev-Gauss-Lobatto points may be used to that end, it is detrimental for the quality of the results expected to apply the same distribution at the far field, where it is not needed, while the sparsity of the Chebyshev points in the center of the domain may result in inadequate resolution of this region. One possible solution is to use stretching, so that the nodes get concentrated around a desired target region. In this case the goal is to transform the initial domain $I = [-1,1]$ into $A = [a,b]$ with the special feature that the middle point, zero, turns into an arbitrary $y_{1/2} \in [a,b]$.

So let $x_i = \cos\frac{i\pi}{N}$, the stretching function,

$$f(x_i) = a + \frac{\frac{(b-a)(y_{1/2}-a)}{b+a-2y_{1/2}}(1+x_i)}{\frac{2(y_{1/2}-a)}{b+a-2y_{1/2}} + (1-x_i)} \tag{53}$$

transform every point in x_i into A, such that, $f(-1) = a$, $f(1) = b$ and $f(0) = y_{1/2}$.
This function could also be written as:

$$f(x_i) = a + \frac{c(b-a)(1+x_i)}{(1-2\cdot c)(1-x_i)}$$

where c is a stretching factor and represents the displacement ratio of the image of $x_i = 0$ in A. This function is not continuous when $y_{1/2} = (b+a)/2$; $c = 0.5$, i.e. when there is no stretching.

For representing a function u in the new set of points y_i in A, the procedure is the same than for any mapping, taking into account that,

$$f^{-1}(y_i) = \frac{(2\cdot c+1)(y_i-a) - (b-a)c}{(b-a)c + (y_i-a)}$$

and its derivatives could be easily calculated.

3.1.4 Two–dimensional expansions

All the one-dimensional results presented up to this point can be extended to the multidimensional approach.
The extension to two dimensional approximations is done using tensor products of one-dimensional expansions. Thus in the unit square $[-1,1]^2$ and for Chebyshev polynomials,

$$T_{ij}(x,y) \equiv T_i(x)T_j(y) \quad i = 1,\ldots,N_x; j = 1,\ldots,N_y \tag{54}$$

The truncated Chebyshev series of degree N_x in the x-direction and N_y in the y-direction is

$$\begin{aligned} u_{\mathcal{N}}(x,y) &= \sum_{i=0}^{N_x}\sum_{j=0}^{N_y} \hat{u}_{ij}T_i(x)T_j(y) \\ &= \sum_{i=0}^{N_x}\sum_{j=0}^{N_y} \hat{u}_{ij}T_{ij}(x,y) \end{aligned} \tag{55}$$

Orthogonality of each one-dimensional Chebyshev basis implies orthogonality of the tensor product two-dimensional basis.

$$(T_{km}, T_{ln})_w = \frac{\pi^2}{4} c_k c_m \delta_{k,l}\delta_{m,n}$$

The approximation of a function $u(x,y)$ with the collocation technique makes use of the Gauss or Gauss-Lobatto mesh:

$$ll\left(x_i, y_j\right) = \left(\cos\frac{i\pi}{N}, \cos\frac{j\pi}{N}\right) \quad \text{Gauss-Lobatto choice.} \tag{56}$$

$$\left(x_i, y_j\right) \in \Omega_N = [-1,1]\times[-1,1] \tag{57}$$

This matrix of nodes is arranged in an array fixing the y-value while x-value changes. This choice is the responsible for the characteristic form of differential Chebyshev pseudo-spectral matrix in each direction.
These matrices can be formed from the 1D differential operator placing every coefficient in its respective row and column or easily if Kronecker tensor product $(\otimes)$ is consider Trefethen (2000) .
The Kronecker product of two matrices A and B of dimension $p \times q$ and $r \times s$ respectively is denoted by $A \otimes B$ of dimension $pr \times qs$. For instance

$$\begin{pmatrix} 1 & 2 \\ 3 & 4 \end{pmatrix} \otimes \begin{pmatrix} a & b \\ c & d \end{pmatrix} = \left(\begin{array}{cc|cc} a & b & 2a & 2b \\ c & d & 2c & 2d \\ \hline 3a & 3b & 4a & 4b \\ 3c & 3d & 4c & 4d \end{array}\right) \tag{58}$$

Using this tensor product, the two dimensional derivatives matrices are computed. Let $[a, b] \times [c, d]$ the computational domain discretized using the same number of Gauss-Lobatto points in each direction (N), and let $\mathcal{D}$ be the one dimensional Chebyshev pseudo-spectral matrix for these number of nodes, then, $\mathcal{D}_x = I \otimes \mathcal{D}$ and $\mathcal{D}_y = \mathcal{D} \otimes I$ where I is the $N \times N$ identity matrix.
Second order derivative matrices are built using the same technique $\mathcal{D}_{xx} = I \otimes \mathcal{D}^2$, $\mathcal{D}_{yy} = \mathcal{D}^2 \otimes I$ and $\mathcal{D}_{xy} = (I \otimes \mathcal{D}) \times (\mathcal{D} \otimes I)$, now it is easy to translate any differential operator to its vector form.

3.1.5 Multidomain theory

Domain decomposition methods are based on dividing the computational region in several domains in which the solution is calculated independently but taking into account information from the neighboring domains. From now on boundary conditions coming from the interface between two domains were called interface conditions to distinguish from physical boundary conditions: inflow, outflow, wall,...
The advantages of this technique appear in several situations. The first one is related with the geometry of the problem to be solved. Chebyshev polynomials, without any metric transformation, require rectangular domains, using this multidomain technique it is possible to deal with problems which can be decomposed into rectangular subdomains. A second advantage of this method is the possibility of mapping specific areas of the computational domain with dense grids while in "less interesting" regions coarse grids could be used. This different resolution for different subdomains allows an accurate solution without wasting computational requirements where not needed.

3.1.6 One-dimensional multidomain method

The multidomain method applied to one dimensional problems means solving as many equations as domains. Due to the choice of Chebyshev-Gauss-Lobatto nodes the domains involved share one extremum point, this node will appear twice in the unknown vector $x_N^1 = x_0^2$.

In vector form for two domains the differential equation would be defined as:

$$\left(\begin{array}{c|c} \mathcal{L}_1 & \\ \hline & \mathcal{L}_2 \end{array}\right)\left(\begin{array}{c} U_1 \\ \\ U_2 \end{array}\right) \tag{59}$$

3.1.7 Two-dimensional multidomain method

It is in the extension to two dimensional problems when the features of the multidomain approach could be better exploited. There is no essential difference with the one–dimensional case but the complexity in the implementation of the technique warrants a detailed explanation.

First the domains are enumerated from bottom to top and from right to left. The connection among them is now not a single point but a row of nodes. In the simplest situation these nodes match between domains, i.e. two domains share a row of nodes. But dealing with problems with "more interesting" regions made necessary the possibility of meshing each domain with a different number of nodes. In this case non-conforming grids are built, which make use of the interpolation tool to be discussed shortly. The matrix form is built in a straightforward manner considering each domain independently.

$$\left(\begin{array}{c|c} \mathcal{L}^1 & 0 \\ \hline 0 & \mathcal{L}^2 \end{array}\right)\left(\begin{array}{c} u^1_{0,0} \\ \vdots \\ u^1_{N_x^1,N_y^1} \\ \hline u^2_{0,0} \\ \vdots \\ u^2_{N_x^2,N_y^2} \end{array}\right) \tag{60}$$

3.1.8 Boundary and interface conditions

Both in one– and two–dimensional problems once the differential matrix has been formed boundary conditions need to be imposed. In multidomain methods two kinds of conditions are present, true *boundary* conditions arising from physical considerations on the behaviour of the sought functions at physical domain boundaries, such as inflow, outflow or wall, and *interface* conditions, imposed in order to provide adequate connection between the subdomains.

3.1.9 One-dimensional boundary and interface conditions

Depending on what kind of boundary condition the problem has (Dirichlet, Neumann, Robin), the implementation is different. The nodes affected by this conditions are, in any type of boundary condition, U_0 and U_N. That is why only the first and last row in the matrix operator are changed, for instance, homogeneous Dirichlet boundary condition in U_0 means

replacing the first row with a row full of zeros but in the first position where will be an one. Neumann bc in U_N needs the substitution of the last row in $\mathcal{L}$ for the last row in $\mathcal{D}$.
Interface conditions in one dimensional problems reduce to imposing continuity equations in the shared node. Depending on the order of the problem the interface continuity conditions are imposed for higher order derivatives. In a second order differential equation, such like the BiGlobal EVPs treated presently, the interface conditions consist of imposing continuity in function and first derivative as follows:

$$\begin{aligned} U_N^1 &= U_0^2 \\ U_N^{1\prime} &= U_0^{2\prime} \end{aligned} \tag{61}$$

The effect on vector form is again the substitution of as much as rows in the matrix as number of conditions needed.

3.1.10 Two-dimensional boundary and interface conditions

After building the matrix which discretized the differential operator, the issue of imposing boundary and interface conditions must be addressed. Boundary conditions do not present additional complexity compared with the one–dimensional case apart from the precise positioning of the coefficient in the matrix; however, interface conditions deserve a more detailed discussion.
The equations for the interface conditions in a two dimensional second order differential problem are the same that the ones for one dimensional case except for the number of nodes involved. If the grids in the two domains are conforming (point to point matching) these equation are (supposing connection between domains in x_{max}^1 to x_{min}^2):

$$\begin{aligned} U^1_{N_x,i} &= U^2_{0,i} \\ \left.\frac{\partial U^1}{\partial x}\right|_{N_x,i} &= \left.\frac{\partial U^2}{\partial x}\right|_{0,i} \end{aligned} \tag{62}$$

If non-conforming grids are present an interpolation tool is necessary for imposing interface conditions. Hence supposing connection between domains in y_{max}^1 to y_{min}^2:

$$\begin{aligned} U^1_{j,N_y} &= \overset{2\to1}{I}_{j,i} U^2_{i,0} \\ \overset{1\to2}{I}_{j,i} \left.\frac{\partial U^1}{\partial y}\right|_{i,N_y} &= \left.\frac{\partial U^2}{\partial y}\right|_{j,0} \end{aligned} \tag{63}$$

3.2 Galerkin approximation method

Turning to the Galerkin approach, the approximate solution of the problem is sought in a function space consisting of sufficiently smooth functions satisfying the boundary conditions. This method is based on the projection of the approximate solution in a finite dimensional

space of the basis functions, ψ. If $(\hat{u}_i, \hat{p})$ is the approximate solution of the problem then:

$$A \begin{pmatrix} \hat{u}_1 \\ \hat{u}_2 \\ \hat{u}_3 \\ \hat{p} \end{pmatrix} + \omega B \begin{pmatrix} \hat{u}_1 \\ \hat{u}_2 \\ \hat{u}_3 \\ \hat{p} \end{pmatrix} = R. \tag{64}$$

where now R is the residual or error that results from taking the approximate numerical solution instead of the exact solution. The residual is projected on a finite basis $\psi_j \quad j = 1, ...N$ with dimension N and the objective of the methodology is to drive R to zero.

$$\int_\Omega R\psi_j d\Omega = \int_\Omega \left[A \begin{pmatrix} \hat{u}_1 \\ \hat{u}_2 \\ \hat{u}_3 \\ \hat{p} \end{pmatrix} + \omega B \begin{pmatrix} \hat{u}_1 \\ \hat{u}_2 \\ \hat{u}_3 \\ \hat{p} \end{pmatrix} \right] \psi_j d\Omega = 0. \tag{65}$$

The operator A contains second derivatives in the viscous term and also the pressure gradient term, for those terms integration by parts must be applied taking into account the boundary conditions. The application of boundary condition vanish boundary integrals where Dirichlet boundary conditions are fixed and also boundaries where natural boundary conditionsGonzález & Bermejo (2005) are imposed.
The approximate solution $(\hat{u}_1, \hat{u}_1, \hat{u}_1, p)$ can be expressed as linear expansion over the number of degrees of freedom of the system. Let us call N the number of velocity points or degrees of freedom and NL the number of pressure points, then the final solution can be expressed as:

$$\hat{u}_i = \psi_\alpha \hat{u}_i^\alpha \qquad (\alpha = 1, ..., N) \tag{66}$$

$$\hat{p} = \psi_\lambda \hat{p}^\lambda \qquad (\lambda = 1, ..., NL) \tag{67}$$

After the variational formulation, the operator A is represented by a $(3N + NL)^2$ matrix, becomes

$$A = \begin{pmatrix} F_{ij} + C_{ij}^{11} + i\beta E_{ij} & C_{ij}^{12} & 0 & -\lambda_{ij}^x \\ C_{ij}^{21} & F_{ij} + C_{ij}^{22} + i\beta E_{ij} & 0 & -\lambda_{ij}^y \\ C_{ij}^{31} & C_j^{32} & F_{ij} + i\beta E_{ij} & i\beta D_{ij} \\ \lambda_{ji}^x & \lambda_{ji}^y & i\beta D_{ji} & 0 \end{pmatrix}, \tag{68}$$

where $F_{ij} \equiv \gamma_{ij} + \left(R_{ij} + \beta^2 M_{ij} \right)$. The real symmetric operator B is also introduced by

$$B = \begin{pmatrix} M_{ij} & 0 & 0 & 0 \\ 0 & M_{ij} & 0 & 0 \\ 0 & 0 & M_{ij} & 0 \\ 0 & 0 & 0 & 0 \end{pmatrix}, i, j = 1, \cdots, N \tag{69}$$

where M represents the mass matrix; the elements of all matrices introduced in (68) and (69) are presented next.
Defining the quadratic velocity basis functions as ψ and the linear pressure basis functions as ϕ, the following entries of the matrices A and B of the generalized BiGlobal EVP appearing in equation (65) are obtained

$$\gamma_{ij} = \bar{u}_m^l \int_\Omega \psi_l \frac{\partial \psi_i}{\partial x_m} \psi_j d\Omega, \qquad l, i, j = 1, ..., N. \tag{70}$$

$$C_{ij}^{mk} = \left(\frac{\partial \bar{u}_m}{\partial x_k} \right)^l \int_\Omega \psi_l \psi_i \psi_j d\Omega, \qquad l, i, j = 1, ..., N \quad m = 1, 2, 3 \quad k = 1, 2. \tag{71}$$

$$E_{ij} = \bar{u}_3^l \int_\Omega \psi_l \psi_i \psi_j d\Omega, \qquad l, i, j = 1, ..., N. \tag{72}$$

$$R_{ij} = \int_\Omega \frac{\partial \psi_i}{\partial x_m} \frac{\partial \psi_j}{\partial x_m} d\Omega, \qquad i, j = 1, ..., N \quad m = 1, 2. \tag{73}$$

$$M_{ij} = \int_\Omega \psi_i \psi_j d\Omega, \qquad i, j = 1, ..., N. \tag{74}$$

$$D_{ij} = \int_\Omega \phi_i \psi_j d\Omega, \qquad i = 1, ..., NL \quad j = 1, ..., N \tag{75}$$

$$\lambda_{ij}^x = \int_\Omega \phi_i \frac{\partial \psi_j}{\partial x}, \qquad i = 1, ..., NL \quad j = 1, ..., N d\Omega, \tag{76}$$

$$\lambda_{ij}^y = \int_\Omega \phi_i \frac{\partial \psi_j}{\partial y}, \qquad i = 1, ..., NL \quad j = 1, ..., N d\Omega. \tag{77}$$

3.2.1 Low-order Taylor-Hood finite elements

Once a general Galerkin formulation of the EVP has been constructed, a choice of a certain base for the basis functions to construct a final version of the operators A and B must be made. All the terms contained in those operators are defined by an integral over the computational domain Ω. To perform the calculation of those integrals we are going to divide the full computational domain into a finite number of sub-domains or elements. Let us call M the number of elements used for the domain decomposition, this implies that a mesh generation has been performed in such a way that:

$$\bigcup_{i=1}^{M} \Omega_i = \Omega, \tag{78}$$

$$\bigcap_{i=1}^{M} \Omega_i = \emptyset, \tag{79}$$

The two-dimensional computational domain will be divided in either triangular or quadrilateral elements. As the integral calculation has been reduced to the summation of integrals over single elements, then the basic functions must be defined in the different

elements. An alternative way is to map all triangular/quadrilateral elements into a standard triangular/element element known as the reference element, this way the definition of the basis functions is only performed once for this reference element.
Before discussing the benefits of different types of polynomial expansions, we first need to introduce the concepts of modal and nodal expansions. In a nodal expansion the value of the coefficients that are used in the linear expansion of the solution are representing the approximate solution in a certain discretization point, this means that the numerical value has a physical interpretation. On the other hand a modal expansion does not have that physical meaning and the physical point comes from the full linear combination of modes.
The numerical solution of the EVPs described in the previous sections may be accomplished by a nodal expansion of the unknowns on a set of nodes, x_q, using a set of basis functions, $\Phi_q(x)$. Linear- and quadratic Lagrange polynomials are the method of choice for $\Phi(x)$ in low-order FEM Cuvelier et al. (1986), and have also been used in our earlier work Gonzalez L et al. (2007). The associated nodal points, x_q, are chosen such that that $\Phi_p(x_q) = \delta_{pq}$, where δ_{pq} represents the Kronecker delta. This property implies that the discrete approximation, u^δ, of a function may be defined at x_q in terms of the expansion coefficients $\widehat{u}_p$ as

$$u^\delta\left(x_q\right) = \sum_{p=0}^{P} \widehat{u}_p \Phi_p(x_q) = \sum_{p=0}^{P} \widehat{u}_p \delta_{pq} = \widehat{u}_q; \tag{80}$$

in other words, the expansion coefficients approximate the function at the set of the nodal points.
One of the typical example of nodal basis functions are the Taylor-Hood elements, this is a P2/P1-quadratic polynomials for velocity and linear polynomials for pressure (or Q2/Q1ÂŮbiquadratic polynomials for velocity and bilinear polynomials for pressure); see Allievi & Bermejo (2000); González & Bermejo (2005) for further details. This configuration ensures stability of the finite-element discretization of all EVPs solved, the $inf - sup$ compatibility condition must be satisfied by the discrete spaces in which disturbance velocity components and disturbance pressure are respectively discretized.
However, experience with the low-order method has shown that the necessity to resolve structures associated with linear perturbations at moderate $Re-$numbers results in the need for rather fine grids, with all the consequent large memory and CPU time requirements Gonzalez L et al. (2007). It is then natural to seek an alternative high order discretization, based on a modal expansion.

3.2.2 High order spectral/hp elements

The first characteristic of such an expansion is that there is no physical interpretation of the associated expansion coefficients. Second, modal expansion is hierarchical, meaning that the expansion set of order $P-1$ is contained within the expansion set of order P; a modal expansion based on the Legendre polynomials $L_p(x)$ will be used in what follows. The key property of this expansion set is its orthogonality which, in addition to the hierarchical construction, leads to well-conditioned matrices Karniadakis & Sherwin (2005). Note that, for problems involving up to second-order differentiation, as those encountered herein, it is sufficient to guarantee that the approximate solution is in H^1. Typically, in the finite element methods this is solved imposing a C^0 continuity between elemental regions, that is the global

expansion modes are continuous everywhere in the solution domain while continuity in the derivatives is achieved at convergence Karniadakis & Sherwin (2005). Boundary and interior nodes are distinguished in this expansion: the former are equal to unity at one of the elemental boundaries and are zero at all other boundaries; the latter class of modes are non-zero only at the interior of each element and are zero along all boundaries. In the standard interval $\Omega = \{\xi | -1 \leq \xi \leq 1\}$ the $p-$type modal expansion is denoted by $\psi_p(x)$ and is defined as

$$\psi_p(\xi) = \begin{cases} \dfrac{1-\xi}{2} & p = 0 \\ \left[\dfrac{1-\xi}{2}\right]\left[\dfrac{1+\xi}{2}\right] L_{p-1}(\xi) & 0 < p < P \\ \dfrac{1+\xi}{2} & p = P \end{cases}$$

It may be seen that the lowest expansion modes, $\psi_0(x)$ and $\psi_P(x)$, are the same as the low-order finite element expansion, these boundary modes being the only modes that are nonzero at the ends of the interval. The remaining interior modes are zero at the ends of the interval and increase in polynomial order. As a consequence of the orthogonality of the Legendre polynomials $L_{p-1}(\xi)$ the stiffness and mass matrices in one-dimensional problems are tri- and penta-diagonal, respectively. The resulting discretization is denoted as spectral/hp element method.

In an one-dimensional spectral/hp decomposition the global expansion basis is decomposed into elemental subdomains that can then be mapped into the standard interval $[-1, 1]$. The polynomial basis is then defined in the standard region. To complete a Galerkin formulation it will be necessary to choose some form of numerical integration; for the purpose of the present work Gaussian quadrature is selected. The one-dimensional concept may be extended to multiple dimensions in a straightforward manner. In two dimensions two standard regions, a quadrilateral or a triangle, may be used. All bases used in what follows can be expressed in terms of modified principal functions. In the quadrilateral expansion:

$$\psi_{pq}(\xi_1, \xi_2) = \psi_p(\xi_1)\psi_q(\xi_2). \tag{81}$$

In the triangular expansion:

$$\psi_{pq}(\xi_1, \xi_2) = \psi_p(\eta_1)\psi_{pq}(\eta_2). \tag{82}$$

In the standard quadrilateral region, the Cartesian coordinates (ξ_1, ξ_2) are bounded by constant limits

$$\mathcal{Q}^2 = \{(\xi_1, \xi_2) | -1 \leq \xi_1, \xi_2 \leq 1\}. \tag{83}$$

This is not the case in the standard triangular region, where the bounds of the Cartesian coordinates (ξ_1, ξ_2) depend on each other, that is,

$$\mathcal{T}^2 = \{(\xi_1, \xi_2) | -1 \leq \xi_1, \xi_2, \xi_1 + \xi_2 \leq 0\}. \tag{84}$$

A means of developing a suitable tensorial-type basis within unstructured regions, such as the triangle, is suggested by Karniadakis and Sherwin Karniadakis & Sherwin (2005),

in terms of a coordinate system in which the local coordinates have independent bounds. The advantage of such a system is that one-dimensional functions may be defined, upon which a multi-domain tensorial basis may be constructed. A suitable coordinate system, which describes the triangular region between constant independent limits, is defined by the transformation Karniadakis & Sherwin (2005)

$$\eta_1 = 2\frac{1+\xi_1}{1-\xi_2} - 1, \tag{85}$$

$$\eta_2 = \xi_2. \tag{86}$$

The final step in constructing a multi-dimensional spectral/hp approximation is a mapping of every subdomain (element) into the corresponding standard region $[-1,1]$ for the 1-D case, $\mathcal{Q}^2$ for the 2-D quadrilateral elements or $\mathcal{T}^2$ for the 2-D triangular elements.
In order to ensure stability of the finite-element discretization of all EVPs solved, the $inf-sup$ compatibility condition must be satisfied by the discrete spaces in which disturbance velocity components and disturbance pressure are respectively discretized. In the present spectral/hp solution the number of disturbance pressure modes has been kept one less than that of the disturbance velocities.

4. EVP solution – Krylov subspace iteration

Having dealt with the spatial discretization of the EVP, we now turn our attention to obtaining the eigenvalues of the LNSE direct or adjoint matrix. From a linear stability analysis point of view, the most important eigenvalues are those closest to the axis $\omega_r = 0$ and here an iterative method has been used for their determination. Specifically, the well-established in BiGlobal linear instability problemsTheofilis (2003) Arnoldi algorithm Nayar & Ortega (1993) has been used.
The Arnoldi method is a subspace iteration method, the computation time of which depends linearly on the subspace dimension. As experienced in earlier analogous studiesDing & Kawahara (1998) only eigenvalues with large modules can be obtained by straightforward application of the algorithm. Since the eigenvalues closest to the imaginary axis are sought, a simple transformation is used in order to convert the original problem into one where the desired values have large modules. Note that the eigenvectors are not affected by this transformation. Specifically, defining

$$\mu = -\omega^{-1}, \tag{87}$$

it follows that

$$A^{-1}B\hat{\mathbf{q}} = \mu\hat{\mathbf{q}}, \quad A^{-1}B = C, \quad C\hat{\mathbf{q}} = \mu\hat{\mathbf{q}}. \tag{88}$$

This transformation converts the original generalized into the standard EVP. A finite but small (compared with the leading dimension of A, B) number of eigenvalues (equal to the Krylov subspace dimension) m is sought, which is obtained by application of the Arnoldi algorithm as follows

1. CHOOSE an initial random vector v_1 and NORMALIZE it.
2. FOR j=1,2,....m DO:
   (a) Calculate w_j as $Cv_j = w_j$. Which is equivalent to solve the problem $Aw_j = Bv_j$(A non-symmetric).
   (b) FOR i=1,2,...j DO:

$$h_{ij} = (Cv_j, v_i), \tag{89}$$

$$a = \sum_{i=1}^{j} h_{ij} v_i, \tag{90}$$

$$\hat{v}_{j+1} = w_j - a, \tag{91}$$

$$h_{j+1,j} = \|\hat{v}_{j+1}\|, \tag{92}$$

$$v_{j+1} = \frac{\hat{v}_{j+1}}{h_{j+1,j}} \tag{93}$$

   END DO
END DO

This algorithm delivers an orthonormal basis $\mathbf{V}_m = [v_1, v_2, ..., v_m]$ of the Krylov subspace $\mathbf{K}_m = span\{v_1, Cv_1, ..., C^{m-1}v_1\}$. The restriction from $\mathbf{C}$ to $\mathbf{K}_m$ is represented by the matrix $\mathbf{H}_m = \{h_{ij}\}$. The eigenvalues of the latter matrix are an approximation of the m largest eigenvalues of the original problem (65). The eigenvectors associated with these eigenvalues may be obtained from

$$\hat{\mathbf{q}}_i = \mathbf{V}_m \tilde{y}_i \tag{94}$$

where $\tilde{y}_i$ is an eigenvector of $\mathbf{H}_m$ associated with the μ_i-th eigenvalue.
Note that, since the matrix C is unknown a-priori, a non-symmetric linear system $Cv_j = A^{-1}Bv_j = q_j$ or, equivalently, $Aq_j = Bv_j$ must be solved at each iteration, q_j being an unknown auxiliary vector. It is important to remark that the invert process needs the inversion of the A operator which means that at least one LU or Incomplete-LU decomposition must be done.
The total time needed for a complete Arnoldi analysis depends mostly on the efficiency of the linear solver described above, as well as on the Krylov space dimension m used to approximate the most important eigenvalues.
In order to find the leading eigenvalue with maximum real part, one can use the shift and invert strategy. If ω_0 is an approximation to the complex eigenvalue of interest, the shifted and inverted problem is

$$(C - \omega_0)^{-1} \hat{\mathbf{q}} = \mu \hat{\mathbf{q}} \tag{95}$$

where $\mu = -(\omega - \omega_0)^{-1}$.

5. Results

5.1 Single–domain spectral collocation computations

Selected results, representative of the applications to which the tools discussed earlier have been applied, are briefly exposed next; full discussion of the respective applications may

be found in the references provided. Starting with the single–domain spectral collocation method on a rectangular domain, which has been the main approach applied to the solution of the BiGlobal EVP by several authors Lin & Malik (1996a;b); Tatsumi & Yoshimura (1990); Theofilis et al. (2003), attention is focused on the global instability of laminar separation bubbles (LSBs) in the incompressible regime Theofilis et al. (2000), and on attachment–line instability in compressible flow Duc et al. (2006); Theofilis, Fedorov & Collis (2004).

In the context of LSB flows, two approaches have been followed for the construction of the basic flows, firstly an analytical one, making use of the attached and the separated Falkner–Skan branches, and secondly an inverse boundary–layer method, in which the wall–shear is prescribed. In the context of the first methodology, the instability analysis was performed for bubbles with different Reynolds numbers, but the same value of $m_{\rm lim} = -0.025$. All the bubbles analyzed have a peak reversed-flow higher than 10% of the reference velocity, chosen in order to ensure proximity to conditions of amplification of the global mode Theofilis et al. (2000). The amplitude functions of the global modes discovered in our previous work were centered on the bubble and extended for only a short distance downstream. Analogous boundary conditions were imposed here but substantially higher resolutions were required in order to converge results at (displacement–thickness–based) Reynolds number $Re = 50$. Concretely, the system (30-33) been solved for the determination of the (direct) linear global perturbations and convergence of the results has been attained using $(N_x, N_y) = (120, 40)$ spectral collocation points and a constant Krylov subspace dimension of 200. At these parameters the discretized eigenvalue problem for each pair of the parameters (Re,β) required the storage and inversion of a matrix with leading dimension 1.98×10^4, which translates on 6 Gbytes of memory. Though hardware was available in order to perform this work serially in a shared–memory manner, all computations shown were performed in parallel.

The spanwise wavenumber parameter range $0 \approx \beta \leq 35$ has been examined and two global modes have been identified. The first one is known from previous work Theofilis et al. (2000), is steady ($\omega_r = 0$) and its periodicity length in the spanwise direction is approximately the same of the bubble; at relatively high β values this mode is transformed into two travelling modes ($\omega_r \neq 0$). The newly discovered mode is always a traveling instability with spanwise periodicity length about a third of that of the bubble Rodríguez (2008). Both modes have been encountered for Reynolds numbers, based on the displacement-thickness at inflow, below 100. On the other hand, the solution of the adjoint BiGlobal EVP provides the spatial regions where the receptivity of the basic flow to small perturbations is higher: the adjoint eigensolution field defines the efficiency by which a particular forcing excites the direct eigensolution Hill (1992). The adjoint BiGlobal EVP (39-42) has been solved next; the boundary conditions applied to the direct problem are inverted here, as discussed in section 2. Dirichlet homogeneous boundary conditions are imposed at the right-hand boundary while linear extrapolation from the interior of the domain is imposed at the left. The amplitude functions recovered are again centered in the bubble, but this time they are extend upstream. Some perturbation velocity components seem to vanish at the left boundary of the domain.

Performing the same analysis for $Re_{\delta^*} = 500$ at inflow, the eigenspectrum is symmetric, and some branches can be identified corresponding to the global modes. The least stable eigenmode founded here is the same steady mode present at lower Reynolds numbers, and is depicted on figure 2 for the direct and adjoint eigenmodes . Much like the lower–Reynolds number case, the spatial structure of the global modes is centered on the bubble, and extends downstream for the direct eigenfunction and upstream for the adjoint Rodríguez & Theofilis

(2008). Finally, relaxing the homogeneous Dirichlet boundary conditions imposed at the inflow boundary, TS–like disturbances may be obtained.Rodríguez & Theofilis (2010)
Single–domain solutions of the compressible BiGlobal EVP (8) are also slowly finding themselves in the literature Robinet (2007); Theofilis & Colonius (2004); Theofilis, Fedorov & Collis (2004). A particularly interesting example is the compressible analogue of the classic swept Hiemenz flow, the global instability of which has been addressed by Lin and Malik Lin & Malik (1996a;b) and further analyzed by Theofilis *et al.* Theofilis et al. (2003). From a numerical point of view, an interesting aspect of this flow is the polynomial structure of its linear global eigenmodes, which is exact in the incompressible limit Theofilis et al. (2003). Recovery of the polynomial structure in the global eigenspectrum is a rather stringent test for the accuracy of any BiGlobal EVP solver. Linear extrapolation has been imposed as a boundary condition on the eigenvector–solution of (8) at $x \to \infty$, along the chordwise direction normal to the attachment–line, *for all* eigenmodes. Although such a boundary condition is exact only for the polynomials depending linearly on the chordwise coordinate x, this boundary condition has been found to perform well for all flow eigenmodes. It was found Theofilis, Fedorov & Collis (2004) that the polynomial structure of the global flow eigenmodes persists in the compressible flow regime in an approximate sense, the error of the approximation being of $O(Ma^2/Re^2)$. The Göertler-Häemmerlin structure of the leading eigenmode, Theofilis, Fedorov & Collis (2004), has been confirmed independently by direct numerical simulations of Le Duc *et al.* Duc et al. (2006). The interested reader is referred to Duc et al. (2006); Lin & Malik (1996a;b); Theofilis, Fedorov & Collis (2004); Theofilis et al. (2003) for more details of global instability analysis of this technologically important flow.
Remaining within the realm of single–domain compressible global linear flow instability, attention is turned to the numerical solution of the inviscid equation (11). The first configuration to be addressed in this context has been the elliptic cone at an angle of attack Theofilis (2001); here, validation results in the Poisson limit of (11) and instability analysis results of an aspect ratio 4 elliptic cone, schematically depicted in figure 3, are briefly discussed. A cut plane parallel to the cone base at a distance $z_0 = 0.5$ from the cone base results in an ellipse with geometric parameters

$$a = 0.5,\ b = 0.125,\ \xi_w \approx 0.255, \tag{96}$$

while $\xi_\infty = 1.5$ has been taken to truncate the integration domain. Several validation and verification problems have been solved in the Poisson and Helmholtz limits of (11), in order to demonstrate exponential convergence of the discretization algorithms on the elliptic confocal grid Theofilis (2001). The standard Chebyshev spectral collocation domain discussed in section 3.1 has been used in the wall–normal direction, while Fourier collocation has been used as the natural choice to discretize the azimuthal spatial direction; both collocation discretizations have been modified in order to introduce the elliptic confocal coordinate system. The convergence history of the results for the wall value $f(x = a, y = 0) = f(\xi = \xi_w, \eta = 0)$, obtained from numerical solution of the Neumann problems defined in Theofilis (2001; 2009a), is presented in table 1 to within six significant digits, while the convergence history of the numerical solution of problems S and A is presented in figure 4; the spatial distribution of $f(x, y)$ for both Dirichlet and Neumann boundary data can be found in the same figure (b).

$N\xi$	$N\eta$	$f_{\mathrm{H}}(x=a,y=0)$	$f_{\mathrm{S}}(x=a,y=0)$	$f_{\mathrm{A}}(x=a,y=0)$
10	10	-0.901970	-1.360926	-0.863940
20	20	-0.901970	-1.367825	-0.867146
40	40	-0.901970	-1.375666	-0.868566
80	80	-0.901970	-1.375823	-0.868586

Table 1. Convergence history of numerical solution of the Poisson problems H, S and A, subject to homogeneous Neumann boundary conditions. $N\xi$ and $N\eta$ respectively denote the number of collocation points along the ξ and η coordinate directions.

A key conclusion based on these results is that in all cases studied exponential convergence of the solutions sought has been obtained. The symmetries of the solutions are recovered, rather than being imposed, by the numerical approach taken. Furthermore, when the function sought has a simple, essentially one-dimensional (in ξ) structure, as the case is in problem H, a small number of collocation points suffices to solve the problem monitored and further increases in resolution are unnecessary. This result is attributed to the convergence properties of the Fourier expansion in η and underlines the significance of the choice of the natural elliptic confocal coordinate system for the problem at hand. The low resolution requirements in the η direction in this class of problems, effectively suggesting that the available computing power can be almost exclusively devoted to resolution of the ξ spatial direction, is significant in terms of the ability of the two-dimensional eigenvalue problem to recover results of classic one-dimensional linear theory; in this case the instability mode can be described with a small number of Fourier modes accounting for resolution of the geometry in the lateral (η) direction, while its principal variation is along the wall-normal ξ direction. As the structure of the sought function becomes increasingly more complicated higher resolution is necessary compared with that needed for problem H, although in both problems S and A also exponential convergence has been obtained. However, to the degree that conclusions on the spatial structure of the sought BiGlobal instability modes on the elliptic cone can be drawn upon evidence provided by the numerical solutions of problems A and S, a resolution issue for the inviscid compressible eigenvalue problem may arise if accuracy of the eigenvalue problem results beyond three to four significant digits is necessary, for instance in the case of near-neutral modes.

Turning to hydrodynamic and aeroacoustic instability analyses, the basic state around the elliptic cone has been computed using a standard, second–order accurate aerodynamic solver on a rather fine mesh. The (dominant) basic flow component along the axis generator has then been extracted and equation (11) has been solved at several subsonic and supersonic Mach numbers. The amplitude functions of the disturbance pressure pertaining to the two leading eigenmodes at $Ma = 0.5$ and $Ma = 4$ are shown also in figure 4. Of interest here is the capability of the global instability analysis to recover perturbations of hydrodynamic nature, such as the subsonic modes shown in figure 4, as well as aeroacoustic disturbances, such as the global eigenmodes of supersonic flow also shown in this figure. A full discussion of the physics of these instabilities may be found in Theofilis (2009a).

5.2 Multi–domain spectral collocation computations

In many situations of practical interest, single–domain computations are inappropriate for the analysis of flow instability. One possible solution in such cases is to employ the tools discussed in section 3.1.

Attention is focused on the solution of the incompressible BiGlobal EVP in a simple geometry, namely stable flow in the lid-driven cavity at $Re = 200, \beta = 1$, the instability of which is now well-documented Theofilis (AIAA-2000-1965); Theofilis, Duck & Owen (2004). The minimum nontrivial discretization involves partition of the square into two sub-domains, each of which is discretized independently. In addition, single-domain results were obtained with the reference codede Vicente et al. (2011); Theofilis (AIAA-2000-1965).

Based on the spanwise disturbance amplitude function $\hat{w}(x, y)$ results of the leading eigenmode at $Re = 200, \beta = 1$, shown in the first row of figure 5, and the associated eigenvalue (not presented here), several observations are worthy of mentioning. First, it can be seen that all combinations of domain decomposition examined, at convergence result in the same (stable) mode. Interestingly, the multidomain approach is more efficient than the single-domain computation on both counts of memory requirements and CPU execution time de Vicente et al. (2006); the highest resolved single-domain computation comprises less points than any of the moderately-resolved multidomain computations, and still requires substantially more computing time in order to deliver results of comparable accuracy.

Once the multi–domain BiGlobal solver has been developed, questions regarding flow instability in relatively complex configurations may be addressed. Such a situation arises in flow over an open cavity which contains store models and the influence of the latter on instability characteristics of an empty cavity. The (non–conforming) spectral multi–domain algorithm developed permits defining the simplest model store configuration possible, namely a rectangular object placed inside an open cavity. The stability of this flow has been considered elsewhere de Vicente et al. (2006); here, for brevity, the geometry, mesh and leading eigenmodes of the aforementioned model problem at parameters $Re = 400, \beta = 2\pi$ are shown in figure 6.

5.3 Finite–element global instability analyses

5.3.1 Low–order FEM

Although a great deal of geometric complexity can be dealt with by combinations of the spectral multi–domain methodology and appropriate choices of mapping functions, there exist situations in which this approach becomes cumbersome, on account of its utilizing regular meshes. An unstructured–mesh finite element or spectral element approach then becomes of interest. Such methods have been developed in our group and in what follows the path to building an unstructured–mesh BiGlobal EVP solver is highlighted via a selection of model applications.

Low–order FEM instability analyses, employing the tools of section 3.2.1, have been performed in several applications, discussed in González et al. (2007); they include closed and open systems and rather complex geometries, such as the triangular lid–driven cavity. Here, an additional paradigm is shown, namely instability in a system of two counter-rotating vortices, in which azimuthal spatial periodicity has not been invoked. The basic flow in this case has been obtained by integrating in time the vorticity-streamfunction equations of motion until certain predetermined criteria have been met. The vortex aspect ratio settles to a linear growth after a short initial transient. A BiGlobal instability analysis of the dipole has been

performed, details of which may be found elsewhere González, Gómez-Blanco & Theofilis (2008); the full flowfield composed of a linear superposition of the leading eigenmode upon the basic state at $Re = 3180$ is shown in figure 7. Such structures, qualitatively known from DNS and experiment, may well be confused with nonlinear phenomena; the present analysis is the first of its kind to demonstrate that their origin is a linear (albeit BiGlobal) modal mechanism.

5.3.2 High–order spectral/hp elements Karniadakis & Sherwin (2005)

The main experience obtained from low–order FEM BiGlobal instability analyses is that rather fine meshes are necessary for converged results to be obtained at Reynolds numbers $Re \geq 10^3$. In turn, these translate in large memory and computing time requirements, making the algorithms exposed in section 3.2 the obvious candidate in order to increase efficiency of the computations. Spectral/$hp-$element BiGlobal EVP analyses have been performed initially for several model problems and subsequently for a range of more realistic applications.

First, an isolated Batchelor vortex, the linear instability of which (studied by classic theory Mayer & Powell (1992)) is well understood. On the other hand, low–order FEM analyses of this flow González, Gómez-Blanco & Theofilis (2008) have demonstrated that very fine meshes are necessary for reliable results to be obtained, even for very low $Re = O(10^2)$. In the present spectral/hp context, a large domain compared with the vortex radius was used to make possible the use of Dirichlet boundary conditions in the outer boundary. The mesh has been concentrated in the neighborhood of the basic flow vortex, while very few elements have been found to be necessary in the outer part of the domain. Provided a large Krylov subspace dimension was used, very good agreement with the results presented by Broadhurst *et al.* Broadhurst et al. (2006) could be obtained at $Re = 667$ and $\beta = 2.0$; in figure 8 the axial component of the disturbance velocity of one of the unstable modes (four lobes) can be seen.

Several confined flows have been analyzed next, starting with the well–studied Hagen Poiseuille flow (HPF) in a circular pipe. While from a physical point of view this is probably the most prominent example of failure of modal linear theory to predict transition, the corresponding one-dimensional eigenvalue problem (of the Orr-Sommerfeld class) has been studied exhaustively over the years Lessen et al. (1968); Salwen et al. (1980), thus serving for the present validation work. The analytically-known basic flow, $\bar{u} = 1 - r^2$, has been recovered on the same unstructured mesh as that on which the BiGlobal instability analysis has been performed. The eigenvalues presented by Lessen Lessen et al. (1968) and Salwen Salwen et al. (1980) at four Reynolds numbers have been calculated and excellent agreement with the literature has been obtained; some results are shown in table 2. The corresponding amplitude functions at $Re = 100$ are shown in figure 9; The (rather coarse, but adequate for convergence) mesh utilized is superimposed in these figures, further underlining the power of the spectral/hp method.

While the HPF is a flow with a single basic flow velocity component, along the homogeneous flow direction, z, it is interesting to test the spectral/$hp-$element BiGlobal EVP solver on a problem, which possesses basic flow velocity components only on the plane normal to the $z-$direction and the instability results of which are well–known. The square lid–driven cavity (LDC) is such a problem, having a two-component basic velocity vector, $(\bar{u}(x,y), \bar{v}(x,y), 0)^{\mathrm{T}}$. In order to eliminate potential sources of sub–optimal convergence, the lid velocity is regularized according to Leriche *et al.* Leriche et al. (1998)

Re	frequency	damping rate	frequency	damping rate	
100	0.57256	-0.14714	0.55198	-0.37446	Salwen Salwen et al. (1980)
100	0.57256	-0.14714	0.55198	-0.37446	Lessen Lessen et al. (1968)
100	0.57256	-0.14714	0.55198	-0.37446	present(h=1,p=18)
200	0.64427	-0.12921	0.51116	-0.20266	Salwen Salwen et al. (1980)
200	0.64426	-0.12920	0.51117	-0.20265	Lessen Lessen et al. (1968)
200	0.64526	-0.12920	0.51117	-0.20265	present(h=1,p=20)
300	0.71295	-0.12900	0.56173	-0.16498	Salwen Salwen et al. (1980)
300	0.71295	-0.12907	0.56171	-0.16497	Lessen Lessen et al. (1968)
300	0.71295	-0.12901	0.56172	-0.16497	present(h=1,p=22)
1000	0.84675	-0.07086	0.46916	-0.09117	Salwen Salwen et al. (1980)
1000	0.84675	-0.07086	0.46924	-0.09090	Lessen Lessen et al. (1968)
1000	0.84682	-0.07090	0.46803	-0.09033	present(h=1,p=22)

Table 2. Eigenmodes of Hagen-Poiseuille flow (HPF) at $\beta = 1$ for different Reynolds numbers, obtained on an single element mesh $h = 1$ and p polynomial degree.

$$\bar{u} = (1 - (2x)^{18})^2 \qquad \text{at} \quad y = 1, \tag{97}$$

while $\bar{u} = 0$ on the other three and $\bar{v} = 0$ on all four cavity boundaries.
It is worth noting that regularization of the boundary conditions in the cavity problem is essential in order to obtain a well-posed problem and avoid having to enter into the somewhat artificial debate found in the literature on the critical conditions for instability (c.f. Poliashenko and AidunPoliashenko & Aidun (1995) and related subsequent work) of a singular basic flow. In order to ensure spatial convergence, a collocation Chebyshev spectral code has been used for the baseflow calculations, see details in Theofilis (2003). The mesh considered for this particular case has $[64x64]$ Gauss-Lobato collocation points. The instability analysis mesh comprises five elements $h = 5$ distributed as four trapezoidal elements, around a central square element. Very good agreement has been obtained with the results of the single–domain code Theofilis (AIAA-2000-1965), while the spatial distribution of the amplitude functions of the leading eigenmode in the regularized LDC flow at $(Re, \beta) = (1000, 17)$ is shown in figure 5.
Having demonstrated the high–order spectral/$hp-$element tools on classic academic problems, instability analyses of incompressible flow through two intakes, both having realistic cross-sectional profiles have been performed next. Without reference to concrete applications, representative duct geometries, inspired from motor racing and fighter jets has been selected González, Rodríguez & Theofilis (2008). In order for the analysis to proceed two key assumptions are made. First, flow is taken to be homogeneous along the streamwise spatial direction; second, flow is taken to be laminar and incompressible, driven by a constant pressure gradient along the streamwise spatial direction. First BiGlobal instability analyses have been performed for intake in_1. The Reynolds number in both cases has then been increased up to $Re = 1000$. Figures 10(upper) show the amplitude functions of the disturbance velocity components pertaining to the leading (least damped) eigenmode at $Re = 1000$ and $\alpha = 1$. While the first intake in_1 analyzed had a combination of straight

lines and rounded corners, the second intake in_2 has a completely curved perimeter. In order to perform an accurate calculation the analytical equation that describes the perimeter must be included as input information for the code. The least–stable mode of in_1 can be found in figure 10(lower). The symmetries in these results, existing on account of those of the corresponding basic state, are clearly visible. In line with the Hagen-Poiseuille flow analyzed earlier, these symmetries have not been imposed in the solution of the BiGlobal eigenvalue problem. However, exploitation of the symmetries is one obvious means of reducing the rather demanding memory requirements for the spectral/hp element method solution of the BiGlobal EVP as the Reynolds number increases.

Two more application are highlighted, namely instability of flow around the T106-300 low pressure turbine (LPT) blade Abdessemed et al. (2004; 2006) and that around an aspect ratio 8 ellipse at an angle of attack of 18^o Kitsios et al. (2008), both in incompressible flow. A main difference of the two analyses is that in the former, unlike the tools discussed up to now, in which the matrix has been formed and stored, a time–stepping approach based on the Nektar code Karniadakis & Sherwin (2005) has been used in order to analyze (primary) modal instability of steady basic flow at low Reynolds numbers, $Re \leq 900$, analyze by Floquet theory with respect to three–dimensional instability the flowfield ensuing amplification of the leading eigenmode at $1000 Re 5000$ and perform transient–growth analysis of the flow. On the other hand, instability around the ellipse has been analyzed by constructing an analytic mapping, based on the Joukowski transformation which, in the particular case of the ellipse reduces to the elliptic confocal mapping discussed in section 2.3. In this case the matrix is formed and stored; the analytical mapping makes it rather dense, while at convergence its dimension approaches 1 Tb Kitsios et al. (2008)), such that massive parallelization is the only viable option in order to recover the matrix eigensystem.

Results of the LPT application are discussed in detail by Abdessemed *et al.* Abdessemed et al. (2004; 2006; 2009). Figure 11 (upper-left) shows the leading traveling eigenmode of this flow at chord-based $Re = 890$ Abdessemed et al. (2004), while in the same figure (upper-right) that of steady, $Re = 200$ flow around the ellipse is shown. The qualitative analogies are striking, although it must be borne in mind that the former computations were serially performed on PCs, while for the latter computations $O(1000)$ processors on the Mare Nostrum supercomputer were required; both computations take about one day's computing to converge. Although the time–stepping approach is clearly orders–of–magnitude more efficient that the matrix storage, the latter approach offers access to two– to three orders–of–magnitude more members of the eigenspectrum than the time–stepper does, alongside added flexibility, especially with respect to interchanging various forms of the (compressible or incompressible, viscous or inviscid) LNSE operators; the latter task would imply major changes in the algorithms underlying the time–stepping approach. In the opinion of the authors, when designing a new BiGlobal instability analysis from scratch, provided one has access to supercomputing facilities either the time–stepping or the matrix formation/storage are valid alternatives to be followed. However, when time–periodic states are to be analyzed, the time–stepping approach is the only candidate to be considered. Figure 11 also shows in the lower case the structure of the leading Floquet eigenmode of the time–periodic flow which ensues in the wake of the LPT, at $Re = 2000$, when the eigenmode shown in the upper case has been linearly amplified. The nature of the secondary instability Floquet (BiGlobal) eigenvalue problem, in which a large number of snapshots in time of the time–periodic basic state are treated in a coupled

manner, make storage of the resulting matrix impossible on both present and near–future computing hardware, such that the time–stepping approach first introduced by Barkley and Henderson Barkley & Henderson (1996) and employed to the LPT problem by Abdessemed *et al.* Abdessemed et al. (2006; 2009) are the only viable alternatives in order to pursue this type of analysis.

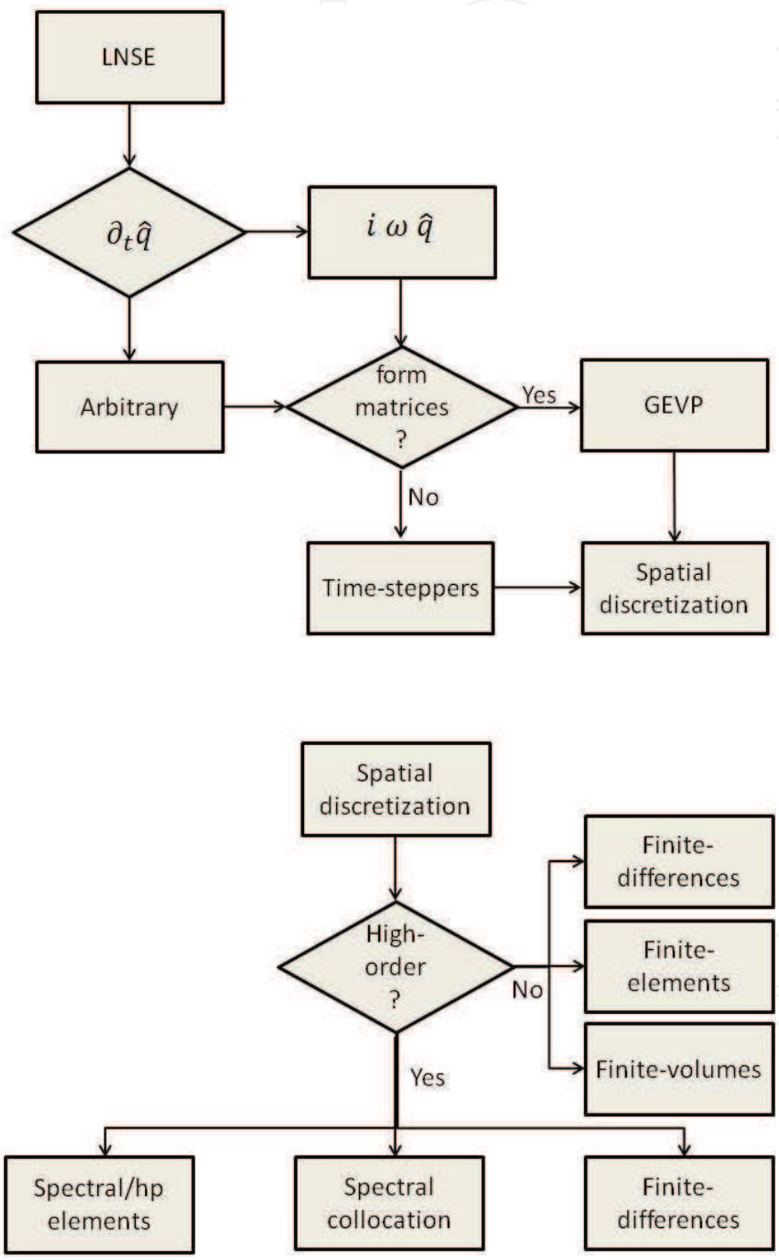

Fig. 1. *Upper:* Treatment of the temporal derivative in a global instability analysis context. *Lower:* Numerical methods which have been used for the spatial discretization of global instability eigenvalue problems.

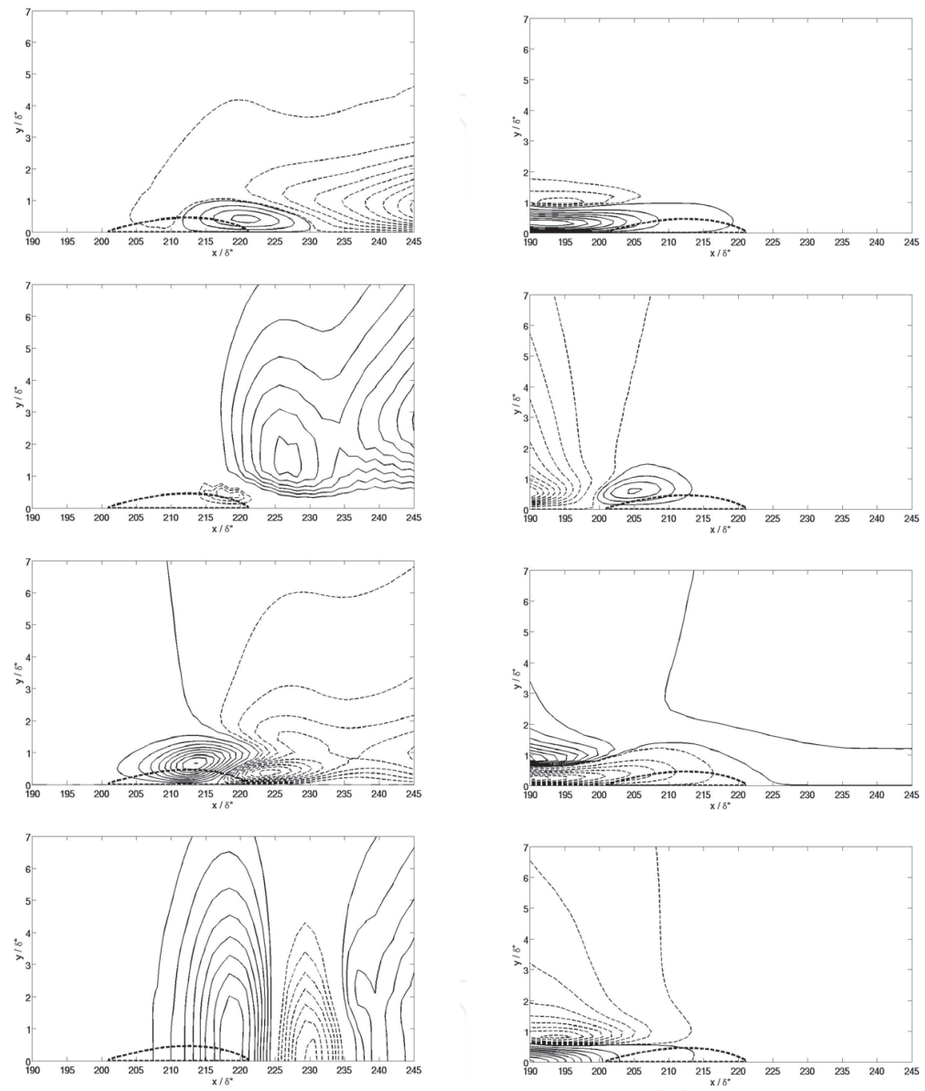

Fig. 2. Most unstable steady global mode for the direct and adjoint problem at $Re_{\delta^*} = 500$ and $\beta = 0.2$. The real streamwise (*first row*), wall-normal (*second row*) and spanwise (*third row*) velocities and pressure (*forth row*) components of the direct (*left column*) and of the adjoint (*right column*) eigenfunctions are shown. The thick dashed line separates the reversed flow region. Only a part of the domain is shown.

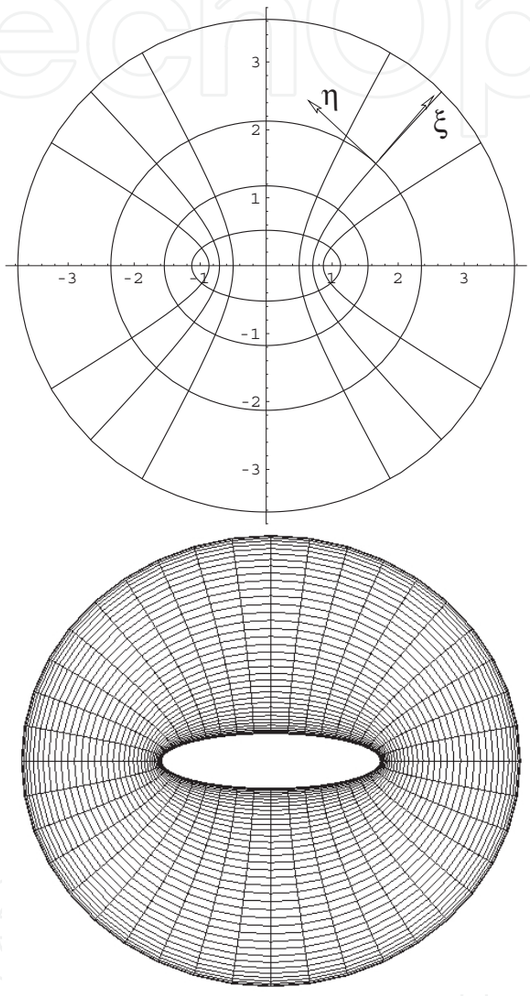

Fig. 3. The elliptic confocal coordinate systemMorse & Feshbach (1953) $O\xi\eta$ (left) and one of the actual grids on which validation work has been performed (right).

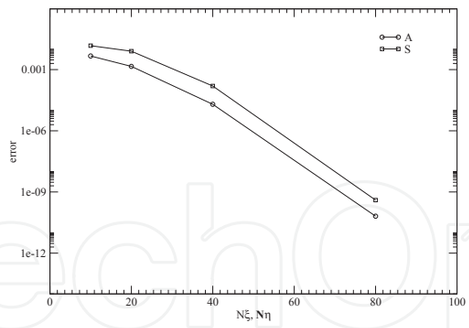

(a)

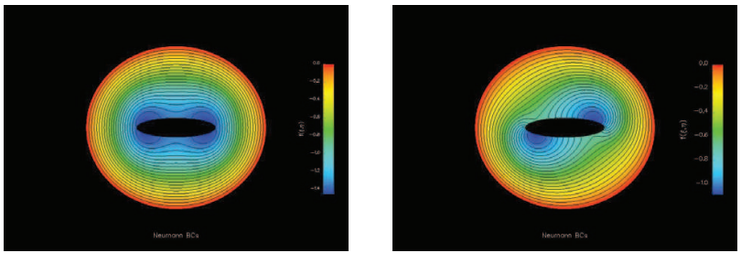

(b)

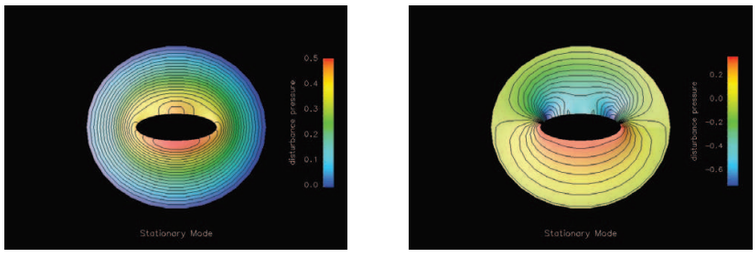

(c)

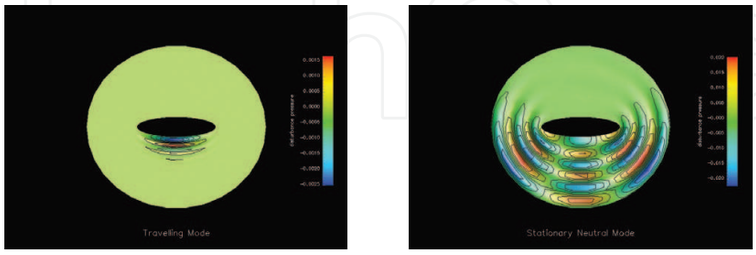

(d)

Fig. 4. (a): Convergence history of the Helmholtz equation on the elliptic confocal grid. (b): Solutions of the Symmetric (left) and Antisymmetric (right) validation problems. (c):Leading eigenmodes of compressible flow over an elliptic cone at $Ma = 0.5$ and (d):$Ma = 4.0$. In (c) and (d) are shown the amplitude functions of the disturbance pressure – solution of (11); first mode in the left– and second mode in the right column.

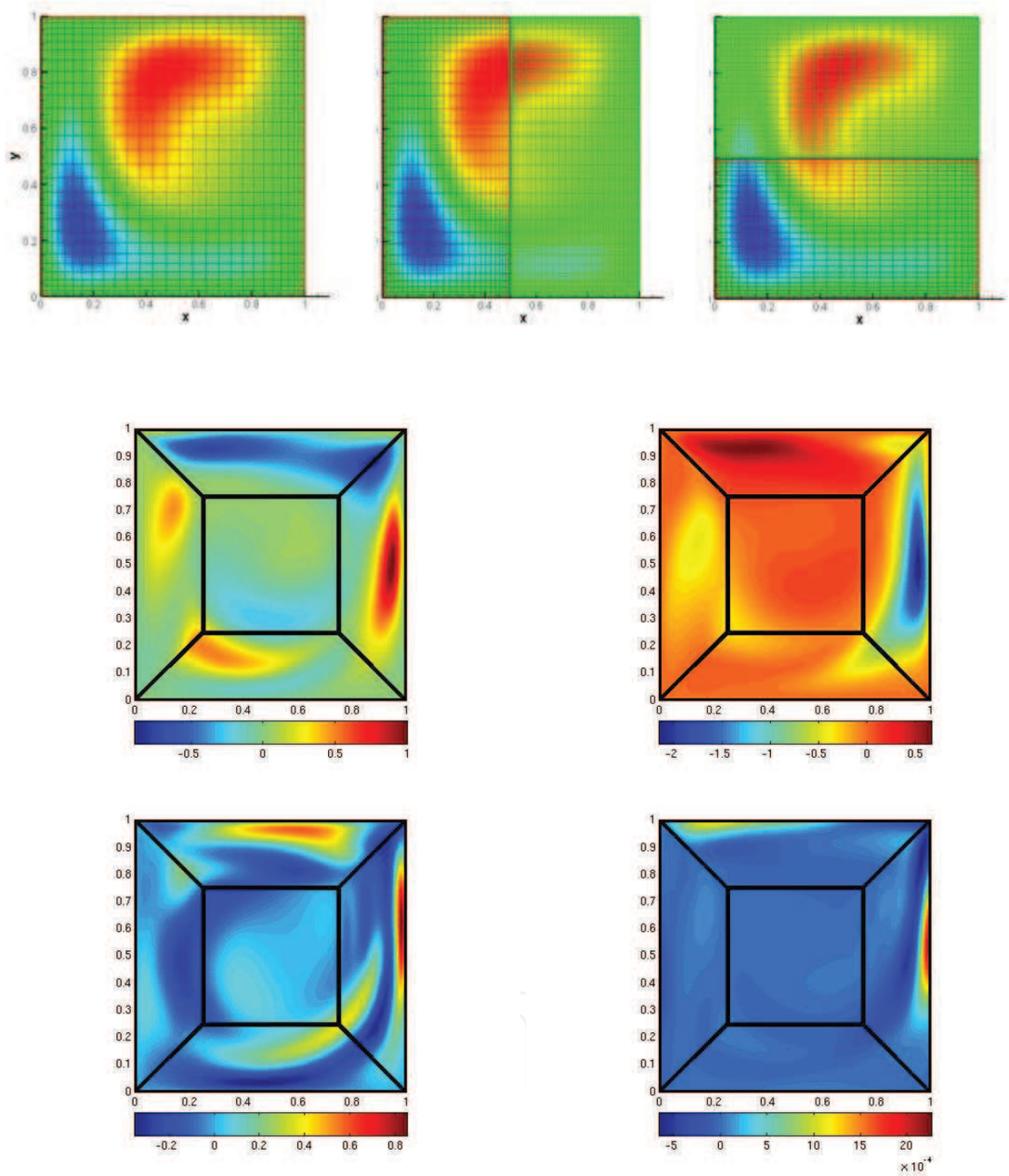

Fig. 5. *Upper:* Amplitude function of the spanwise disturbance velocity component of the least damped eigenmode of lid–driven cavity flow at $Re = 200$ Theofilis (AIAA-2000-1965); Theofilis, Duck & Owen (2004), obtained in single–domain and two different multi–domain configurations with the spectral collocation method. *Lower:* Four components of the most unstable mode of the square cavity flow at Re=1000 $\beta = 17$ obtained using the spectral/$hp-$element method. The mesh used is superposed over the figure.

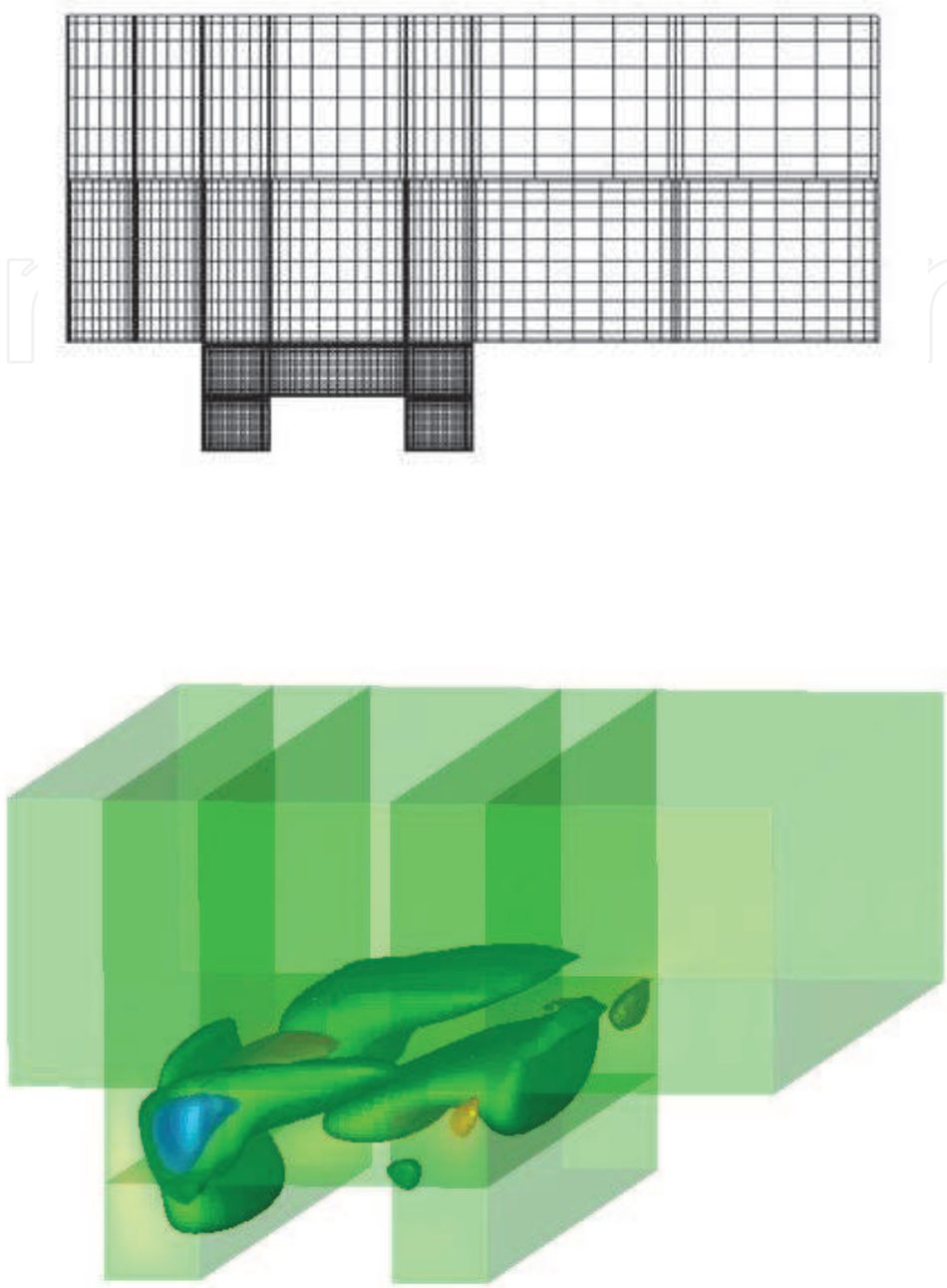

Fig. 6. *Upper:* Non-conforming spectral multidomain discretization of an open–cavity configuration, containing a rectangular object. *Lower:* Perspective view of the least–damped eigenmode of incompressible flow at $Re = 400$ de Vicente et al. (2006).

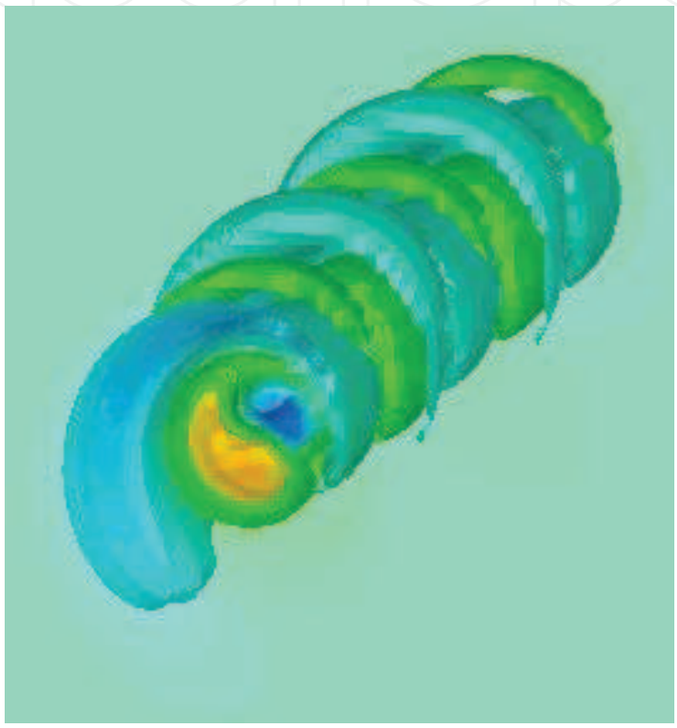

Fig. 7. Superposition upon the steady laminar basic state at $Re = 3180, U_0 = \frac{0.5}{\pi}$, of its most amplified BiGlobal eigenmode at amplitude 0.1%. Axial spatial direction reconstructed using $L_x = 2\pi/\beta$, with $\beta = 3.0$; eigenvalue $\omega_i = 0.04603, \omega_r = 0.06072$ González, Gómez-Blanco & Theofilis (2008).

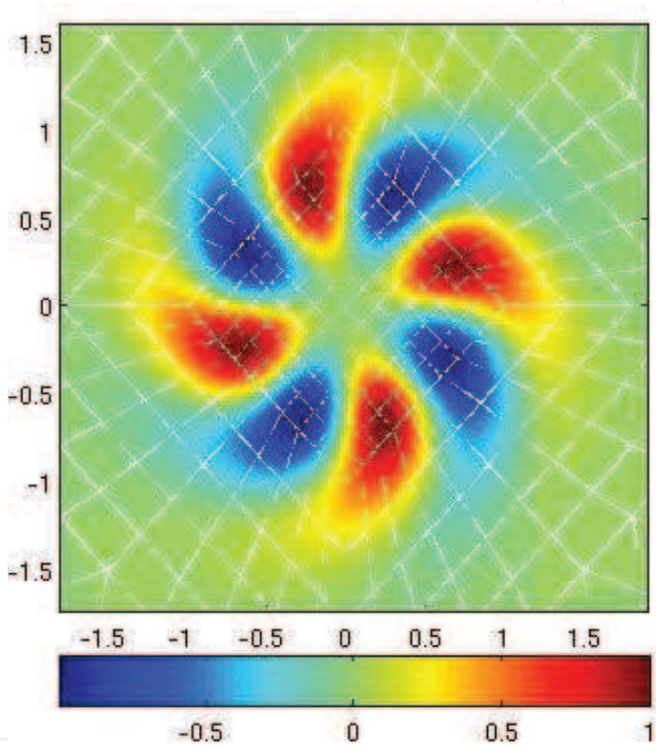

Fig. 8. Axial component of the disturbance velocity of one of the unstable modes(four lobes) of a isolated Batchelor vortex at $Re = 667$ and $\beta = 2.0$.

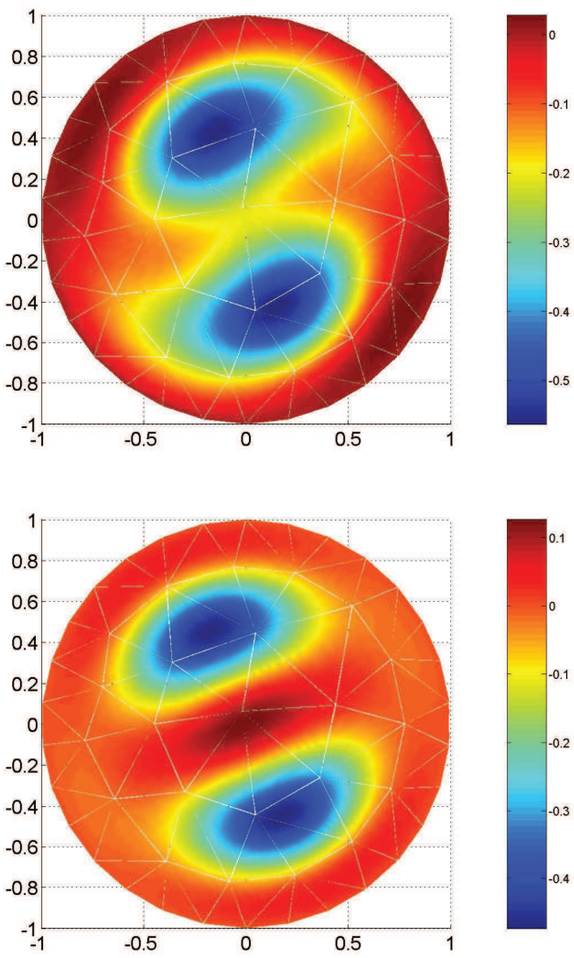

Fig. 9. Leading eigenmodes of HPF flow at $Re = 100, \beta = 1$: shown are the axial disturbance amplitude functions.

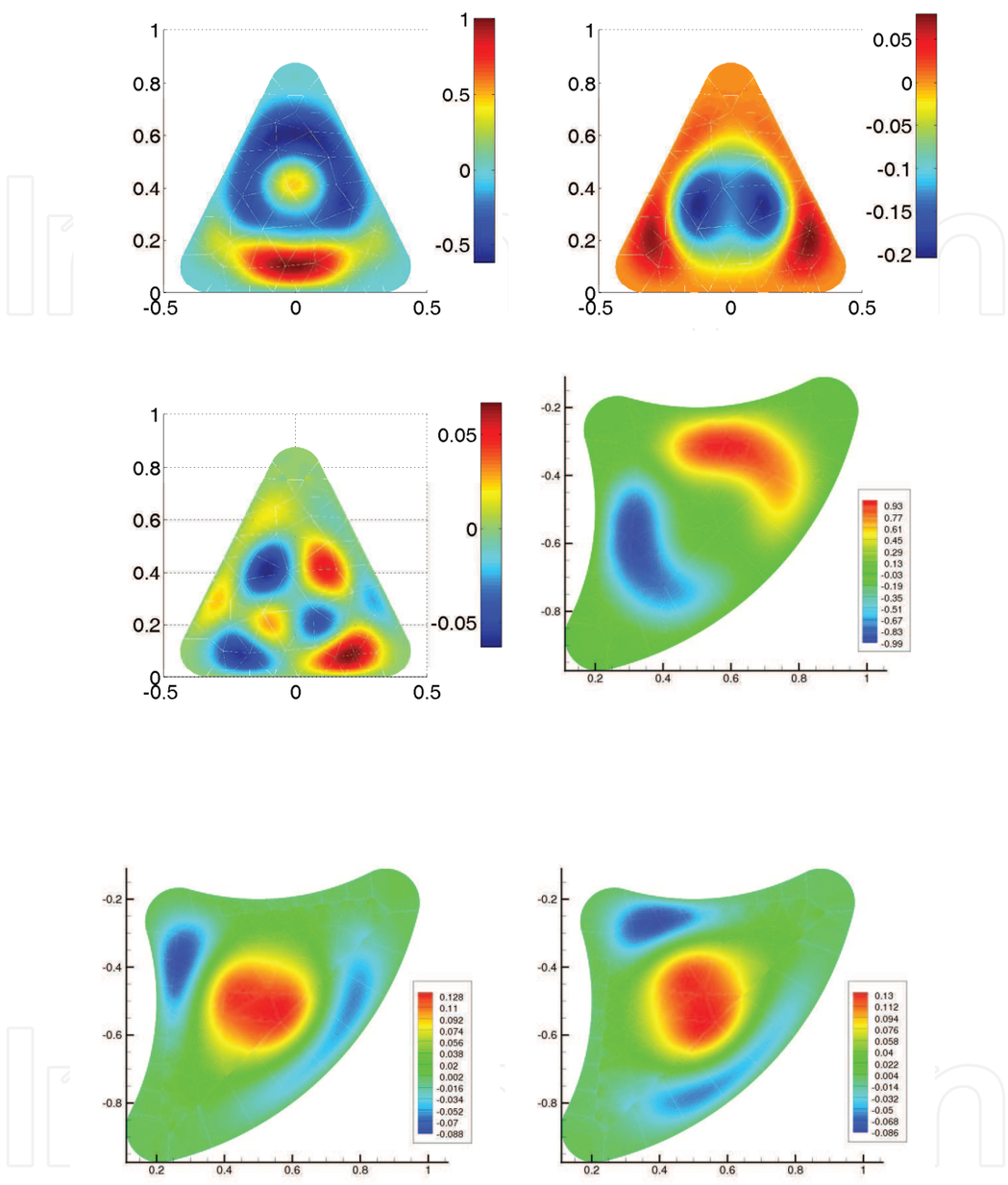

Fig. 10. *Upper:* Amplitude functions of the least-damped eigenmode of geometry "$\mathbf{in}_1$" at $Re = 1000,\ \alpha = 1$ González, Rodríguez & Theofilis (2008).*Lower:* Amplitude functions of the least-damped eigenmode of geometry "$\mathbf{in}_2$" at $Re = 1000,\ \alpha = 1$ González, Rodríguez & Theofilis (2008). Left to right column: $\hat{u}_1,\ \hat{u}_2,\ \hat{u}_3$.

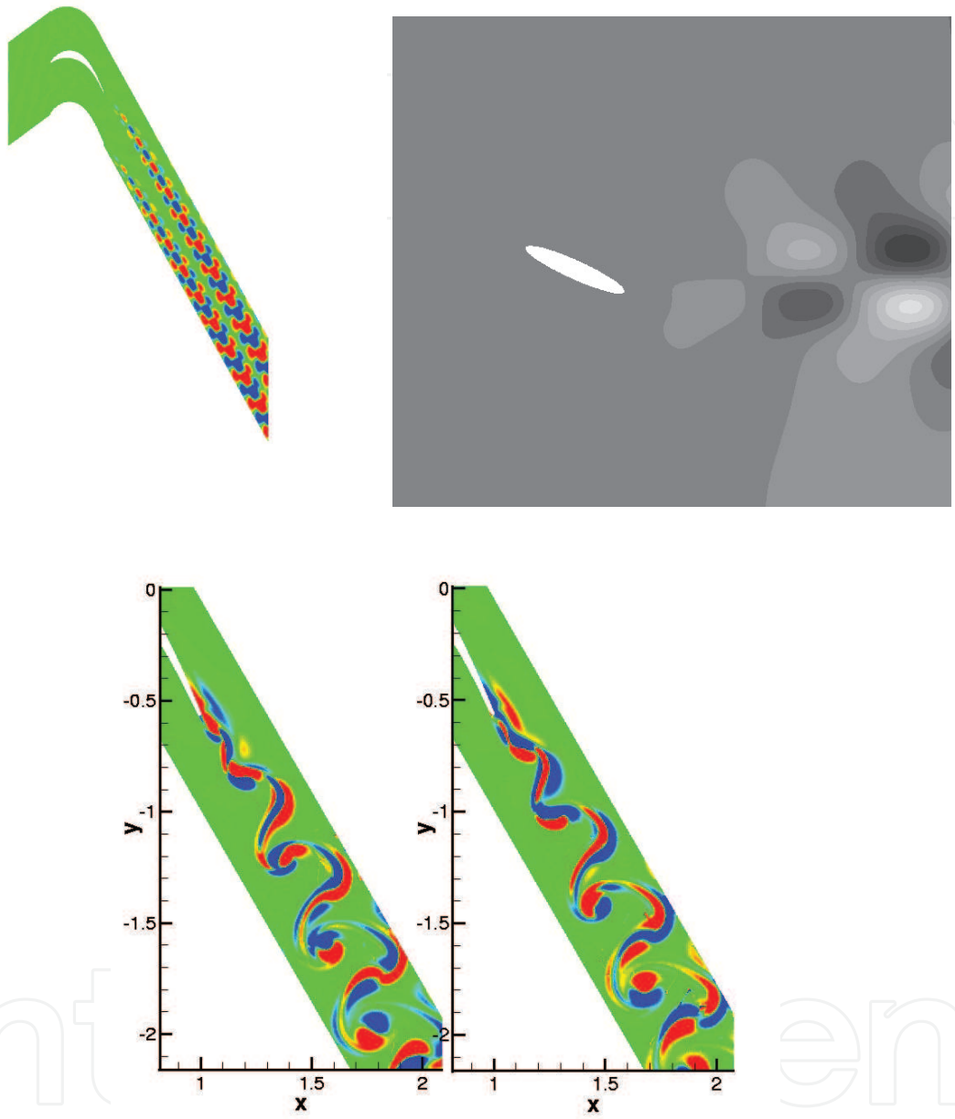

Fig. 11. *Upper-Left:* Leading eigenmode in the wake of the T106-300 LPT flow at $Re = 890$. *Upper-Right:* Leading (wake) eigenmode in flow over an aspect ratio 8 ellipse at $Re = 200$ Kitsios et al. (2008). *Lower:* Leading LPT Floquet mode at $Re = 2000$ Abdessemed et al. (2004).

6. Discussion

Numerical methods for the accurate and efficient solution of incompressible and compressible BiGlobal eigenvalue problems on regular and complex geometries have been discussed. The size of the respective problems warrants particular formulations for each problem intended to be solved: the compressible BiGlobal EVP is only to be addressed when essential compressible flow instability phenomena are expected, e.g. in the cases of shock–induced or supersonic instabilities of hydrodynamic origin or in aeroacoustics research. In all other problems the substantially more efficient incompressible formulation suffices for the analysis. Regarding the issue of time–stepping versus matrix formation approaches, there exist distinct advantages and disadvantages in either methodology; the present article highlights both, in the hope that it will assist newcomers in the field to make educated choices. No strong views on the issue of oder–of–accuracy of the methods utilized are offered, on the one hand because both low– and high–order methods have been successfully employed to the solution of problems of this class and on the other hand no systematic comparisons of the characteristics of the two types of methods have been made to–date. Intentionally, no further conclusions are offered, other than urging the interested reader to keep abreast with the rapidly expanding body of literature on global linear instability analysis.

7. Acknowledgments

The material is based upon work sponsored by the Air Force Office of Scientific Research, Air Force Material Command, USAF, under Grants monitored by Dr. J. D. Schmisseur of AFOSR and Dr. Surya Surampudi of EOARD. The views and conclusions contained herein are those of the author and should not be interpreted as necessarily representing the official policies or endorsements, either expressed or implied, of the Air Force Office of Scientific Research or the U.S. Government.

8. References

Abdessemed, N., Sherwin, S. J. & Theofilis, V. (2004). On unstable 2d basic states in low pressure turbine flows at moderate reynolds numbers, number Paper 2004-2541 in *34th Fluid Dynamics Conference and Exhibit*, AIAA, Portland, Oregon.

Abdessemed, N., Sherwin, S. J. & Theofilis, V. (2006). Linear stability of the flow past a low pressure turbine blade, number Paper 2004-3530 in *36th Fluid Dynamics Conference and Exhibit*, AIAA, San Francisco, CA.

Abdessemed, N., Sherwin, S. J. & Theofilis, V. (2009). Linear instability analysis of low pressure turbine flows, *J. Fluid Mech.* 628: 57 – 83.

Albensoeder, S., Kuhlmann, H. C. & Rath, H. J. (2001a). Multiplicity of steady two-dimensional flows in two–sided lid–driven cavities, *Theor. Comp. Fluid. Dyn.* 14: 223–241.

Albensoeder, S., Kuhlmann, H. C. & Rath, H. J. (2001b). Three-dimensional centrifugal-flow instabilities in the lid-driven-cavity problem, *Phys. Fluids* 13(1): 121–136.

Allievi, A. & Bermejo, R. (2000). A characteristic-finite element conjugate gradient algorithm for the navier-sokes equations, *Int. J. Numer. Meth. Fluids* 32(*): 439–464.

Barkley, D. & Henderson, R. D. (1996). Three-dimensional floquet stability analysis of the wake of a circular cylinder, *J. Fluid Mech.* 322: 215–241.

Bewley, T. R. (2001). Flow control: New challenges for a new renaissance, *Progress in Aerospace Sciences* 37: 21–58.

Bres, G. & Colonius, T. (2008). Three-dimensional instabilities in compressible flow over open cavities, *J. Fluid Mech.* 599: 309–339.

Broadhurst, M., Theofilis, V. & Sherwin, S. J. (2006). Spectral element stability analysis of vortical flows, number Paper 2006-2877 in *6th IUTAM Laminar-Turbulent Transition Symposium*, Bangalore, India, Dec 13–17, 2004, pp. 153–158.

Collis, S. S., Joslin, R. D., Seifert, A. & Theofilis, V. (2004). Issues in active flow control: theory, control, simulation and experiment, *Prog. Aero. Sciences* 40: 237–289.

Crouch, J. D., Garbaruk, A. & Magidov, D. (2007). Predicting the onset of flow unsteadiness based on global instability, *J. Comp. Phys.* 224: 924–940.

Cuvelier, C., Segal, A. & van Steenhoven, A. A. (1986). *Finite Element Methods and Navier-Stokes Equations*, D. Reidel Publishing Company.

de Vicente, J., Rodríguez, D., Theofilis, V. & Valero, E. (2011). Stability analysis in spanwise-periodic double-sided lid-driven cavity flows with complex cross-sectional profiles, *Computers and Fluids* 43: 143–153.

de Vicente, J., Valero, E., González, L. & V.Theofilis (2006). Spectral multi-domain methods for biglobal instability analysis of complex flows over open cavity configurations, number Paper 2006-2877 in *36th AIAA Fluid Dynamics Conference and Exhibit*, AIAA, San Francisco, California.

Ding, Y. & Kawahara, M. (1998). Linear stability of incompressible flow using a mixed finite element method, *J. Comp. Phys.* 139: 243–273.

Dobrinsky, A. & Collis, S. S. (2000). Adjoint parabolized stability equations for receptivity prediction, *AIAA Paper 2000–2651*.

Duc, A. L., Sesterhenn, J. & Friedrich, R. (2006). Instabilities in compressible attachment–line boundary layers, *Phys. Fluids* 18: 044102–1–16.

Giannetti, F. & Luchini, P. (2007). Structural sensitivity of the first instability of the cylinder wake, *J. Fluid Mech.* 581: 167 – 197.

González, L., Gómez-Blanco, R. & Theofilis, V. (2008). Eigenmodes of a counter-rotating vortex dipole, *AIAA J.* DOI: 10.2514/1.35511: to appear.

González, L. M. & Bermejo, R. (2005). A semi-langrangian level set method for incompressible navier-stokes equations with free surface, *Int. J. Numer. Meth. Fluids* 49(*): 1111–1146.

González, L., Rodríguez, D. & Theofilis, V. (2008). On instability analysis of realistic intake flows, number Paper 2008-4380 in *38th Fluid Dynamics Conference and Exhibit*, AIAA, Seattle, WA.

González, L., Theofilis, V. & Gómez-Blanco, R. (2007). Finite element numerical methods for viscous incompressible biglobal linear instability analysis on unstructured meshes, *AIAA J.* 45: 840–855.

Gonzalez L, Theofilis V & Gomez-Blanco R (2007). Finite-element numerical methods for viscous incompressible biglobal linear instability analysis on unstructured meshes, *AIAA Journal* 45(4): 840–855.

Hein, S., Hohage, T., Koch, W. & Schoberl, J. (2007). Acoustic resonances in a high-lift configuration, *J. Fluid Mech.* 582: 179–202.

Henningson, D. S. (1987). Stability of parallel inviscid schear flow with mean spanwise variation, *Tech. Rep. FFA-TN-1987-57*, Bromma, Sweden.

Hill, D. C. (1992). A theoretical approach for the restabilization of wakes, *AIAA Paper 92–0067*.

Karniadakis, G. E. & Sherwin, S. J. (2005). *Spectral/hp element methods for CFD*, OUP.

Kitsios, V., Rodríguez, D., Theofilis, V., Ooi, A. & Soria, J. (2008). Biglobal instability analysis of turbulent flow over an airfoil at an angle of attack, number Paper 2008-4384 in *38th Fluid Dynamics Conference and Exhibit*, AIAA, San Francisco, CA.

Koch, W. (2007). Acoustic resonances in rectangular open cavities, *AIAA J.* 43: 2342–2349.

Leriche, E., Gavrilakis, S. & Deville, M. O. (1998). Direct simulation of the lid-driven cavity flow with chebyshev polynomials, *in* K. D. Papailiou (ed.), *Proc. 4th European Computational Fluid Dynamics Conference*, Vol. 1(1), ECCOMAS, pp. 220–225.

Lessen, M., Sadler, S. G. & Liu, T. Y. (1968). Stability of pipe poiseuille flow, *Phys. Fluids* 11: 1404–1409.

Lin, R.-S. & Malik, M. R. (1996a). On the stability of attachment-line boundary layers. Part 1. the incompressible swept hiemenz flow, *J. Fluid Mech.* 311: 239–255.

Lin, R.-S. & Malik, M. R. (1996b). On the stability of attachment-line boundary layers. Part 2. the effect of leading-edge curvature, *J. Fluid Mech.* 333: 125 – 137.

Mack, L. M. (1984). Boundary layer linear stability theory, *AGARD–R–709 Special course on stability and transition of laminar flow*, pp. 3.1–3.81.

Malik, M. R. (1991). Numerical methods for hypersonic boundary layer stability, *J. Comp. Phys.* 86: 376–413.

Marquet, O., Sipp, D. & Jacquin, L. (2006). Global optimal perturbations in separated flow over a backward-rounded -step, number Paper 2006-2879 in *3rd Flow Control Conference*, AIAA, San Francisco, CA.

Mayer, E. W. & Powell, K. G. (1992). Viscous and inviscid instabilities of a trailing vortex, *Journal of Fluid Mechanics* 245: 91–114.

Morse, P. M. & Feshbach, H. (1953). *Methods of Theoretical Physics, Parts I, II*, McGraw-Hill.

Nayar, N. & Ortega, J. M. (1993). Computation of selected eigenvalues of generalized eigenvalue problems, *J. Comput. Physics* 108: 8–14.

Poliashenko, M. & Aidun, C. K. (1995). A direct method for computation of simple bifurcations, *Journal of Computational Physics* 121: 246–260.

Pralits, J. O. & Hanifi, A. (2003). Optimization of steady suction for disturbance control on infinite swept wings, *Phys. Fluids* 15(9): 2756 – 2772.

Robinet, J.-C. (2007). Bifurcations in shock-wave/laminar-boundary-layer interaction: global instability approach, *J. Fluid Mech.* 579: 85–112.

Rodríguez, D. (2008). On instability and active control of laminar separation bubbles, *Proceedings of the 4th PEGASUS-AIAA Student Conference, Prague* .

Rodríguez, D. & Theofilis, V. (2008). On instability and structural sensitivity of incompressible laminar separation bubbles in a flat–plate boundary layer, number Paper 2008-4148 in *38th AIAA Fluid Dynamics conference, Jan. 23-26, 2008*, AIAA, Seattle, WA.

Rodríguez, D. & Theofilis, V. (2010). Structural changes of laminar separation bubbles induced by global linear instability, *J. Fluid Mech.* p. (to appear).

Sahin, M. & Owens, R. G. (2003). A novel fully-implicit finite volume method applied to the lid-driven cavity problem. part ii. linear stability analysis, *Int. J. Numer. Meth. Fluids* 42: 79–88.

Salwen, H., Cotton, F. W. & Grosch, C. E. (1980). Linear stability of poiseuille flow in a circular pipe, *J. Fluid Mech.* 98: 273–284.

Schmid, P. J. & Henningson, D. S. (2001). *Stability and transition in shear flows*, Springer-Verlag, New York.

Tatsumi, T. & Yoshimura, T. (1990). Stability of the laminar flow in a rectangular duct, *J. Fluid Mech.* 212: 437–449.

Theofilis, V. (2000). Global linear instability in laminar separated boundary layer flow., *in* H. Fasel & W. Saric (eds), *Proc. of the IUTAM Laminar-Turbulent Symposium V*, Sedona, AZ, USA, pp. 663 – 668.

Theofilis, V. (2001). Inviscid gglobal linear instability of compressible flow on an elliptic cone: algorithmic developments, *Technical Report F61775-00-WE069*, European Office of Aerospace Research and Development.

Theofilis, V. (2003). Advances in global linear instability of nonparallel and three-dimensional flows, *Prog. Aero. Sciences* 39 (4): 249–315.

Theofilis, V. (2009a). On multidimensional global eigenvalue problems for hydrodynamic and aeroacoustic instabilities, number Paper 2009-0007 in *47th Aerospace Sciences Meeting 5–8 Jan. 2009*, AIAA, Orlando, FL.

Theofilis, V. (2009b). The role of instability theory in flow control, *in* R. D. Joslin & D. Miller (eds), *Active Flow Control*, AIAA Progress in Aeronautics and Astronautics Series, AIAA.

Theofilis, V. (2011). Global linear instability, *Annu. Rev. Fluid Mech.* 43: 319–352.

Theofilis, V. (AIAA-2000-1965). Globally unstable basic flows in open cavities, *6th AIAA Aeroacoustics Conference and Exhibit* .

Theofilis, V., Barkley, D. & Sherwin, S. J. (2002). Spectral/hp element technology for flow instability and control, *Aero. J.* 106(619-625).

Theofilis, V. & Colonius, T. (2003). An algorithm for the recovery of 2- and 3-d biglobal instabilities of compressible flow over 2-d open cavities, AIAA Paper 2003-4143.

Theofilis, V. & Colonius, T. (2004). Three-dimensional instablities of compressible flow over open cavities: direct solution of the biglobal eigenvalue problem, 34th Fluid Dynamics Conference and Exhibit, AIAA Paper 2004-2544, Portland, Oregon.

Theofilis, V., Duck, P. W. & Owen, J. (2004). Viscous linear stability analysis of rectangular duct and cavity flows, *J. Fluid. Mech.* 505: 249–286.

Theofilis, V., Fedorov, A. & Collis, S. S. (2004). Leading-edge boundary layer flow: PrandtlÂt's vision, current developments and future perspectives, *IUTAM Symposium "One Hundred Years of Boundary Layer Research", Göttingen, Germany, August 12-14, 2004*, Springer, pp. 73–82.

Theofilis, V., Fedorov, A., Obrist, D. & Dallmann, U. C. (2003). The extended görtler-hämmerlin model for linear instability of three-dimensional incompressible swept attachment-line boundary layer flow, *J. Fluid Mech.* 487: 271–313.

Theofilis, V., Hein, S. & Dallmann, U. C. (2000). On the origins of unsteadiness and three-dimensionality in a laminar separation bubble, *Phil. Trans. Roy. Soc. (London) A* 358: 3229–3246.

Trefethen, L. N. (2000). *Spectral Methods in Matlab*, SIAM.

Zhigulev, V. N. & Tumin, A. (1987). Origin of turbulence, *Nauka* .

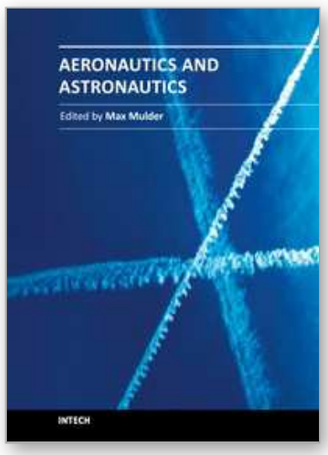

Aeronautics and Astronautics

Edited by Prof. Max Mulder

ISBN 978-953-307-473-3
Hard cover, 610 pages
Publisher InTech
Published online 12, September, 2011
Published in print edition September, 2011

In its first centennial, aerospace has matured from a pioneering activity to an indispensable enabler of our daily life activities. In the next twenty to thirty years, aerospace will face a tremendous challenge - the development of flying objects that do not depend on fossil fuels. The twenty-three chapters in this book capture some of the new technologies and methods that are currently being developed to enable sustainable air transport and space flight. It clearly illustrates the multi-disciplinary character of aerospace engineering, and the fact that the challenges of air transportation and space missions continue to call for the most innovative solutions and daring concepts.

InTech Europe
University Campus STeP Ri
Slavka Krautzeka 83/A
51000 Rijeka, Croatia
Phone: +385 (51) 770 447
Fax: +385 (51) 686 166
www.intechopen.com

InTech China
Unit 405, Office Block, Hotel Equatorial Shanghai
No.65, Yan An Road (West), Shanghai, 200040, China
中国上海市延安西路65号上海国际贵都大饭店办公楼405单元
Phone: +86-21-62489820
Fax: +86-21-62489821

IntechOpen